Foxp3 Orchestrates Reorganization of Chromatin Architecture to Establish Regulatory T Cell Identity

Zhi Liu[1,2,#], Dong-Sung Lee[3,4,#], Yuqiong Liang[1], Ye Zheng[1,*], and Jesse R Dixon[3,*]

1. NOMIS Center for Immunobiology and Microbial Pathogenesis, Salk Institute for Biological Studies, La Jolla, CA, USA
2. Shanghai Immune Therapy Institute, Renji Hospital, Shanghai Jiao Tong University School of Medicine, Shanghai, China
3. Gene Expression Laboratory, Salk Institute for Biological Studies, La Jolla, CA, USA
4. Department of Life Sciences, University of Seoul, Seoul, South Korea

Co-first authors

* Co-corresponding authors

SUMMARY

Chromatin conformation reorganization is emerging as an important layer of regulation for gene expression and lineage specification. Yet, how lineage-specific transcription factors contribute to the establishment of cell type-specific 3D chromatin architecture in the immune cells remains unclear, especially for the late stages of T cell subset differentiation and maturation. Regulatory T cells (Treg) are mainly generated in the thymus as a subpopulation of T cells specializing in suppressing excessive immune responses. Here, by comprehensively mapping 3D chromatin organization during Treg cell differentiation, we show that Treg-specific chromatin structures were progressively established during its lineage specification, and highly associated with Treg signature gene expression. Additionally, the binding sites of Foxp3, a Treg lineage specifying transcription factor, were highly enriched at Treg-specific chromatin loop anchors. Further comparison of the chromatin interactions between wide-type Tregs versus Treg cells from Foxp3 knock-in/knockout or newly-generated Foxp3 domain-swap mutant mouse revealed that Foxp3 was essential for the establishment of Treg-specific 3D chromatin architecture, although it was not dependent on the formation of the Foxp3 domain-swapped dimer. These results highlighted an underappreciated role of Foxp3 in modulating Treg-specific 3D chromatin structure formation.

INTRODUCTION

Genome-wide 3D chromosome conformation capture technologies have revealed that higher-order 3D chromatin structures of mammalian genome are hierarchically organized into chromosome territories, A/B compartments, topologically associating domains (TADs), and chromatin loops[1-5]. TADs are genomic regions that self-interact but insulate regions outside the domain, therefore contributing to the regulation of gene expression by restricting interactions of cis-regulatory elements to their target genes[6-8]. Zinc-finger transcription factor CTCF and the ring-shaped cohesin complex play critical roles in the formation and maintenance of TADs across different cell lineages[9]. However, these ubiquitously expressed proteins alone cannot establish and maintain cell lineage-specific genome architecture. Lineage-specific transcription factors have been proposed to regulate genome organization in specific cell lineages[8,10,11]. As for T cells in the immune system, it has been revealed that Bcl11b and TCF1 controls 3D chromatin architectures during early T cell development[12-14]. However, little is known about global genome organization for the late stage of T cell development and differentiation.

Regulatory T cells (Treg) are a subset of CD4+ T cells subset that suppress excessive immune responses. Treg cell lineage specification represents one of the final stages of T cell development and thus is an excellent model to examine the roles of lineage-specific transcription factors in 3D genome organization[15,16]. Foxp3, an X chromosome-encoded gene in the forkhead transcription factor family, plays a central role in Treg cell lineage specification, phenotypic stability, metabolic fitness, and regulatory function[17-24]. Depending on the activating or repressing cofactors it associates with[21,25], Foxp3 can either promote or inhibit target gene expression by exploiting pre-existing

enhancer landscapes[26]. A recent study using HiChIP showed that Foxp3 was associated with enhancer-promoter loops to fine tune Foxp3-dependent gene expression[27]. However, it remains elusive how the Treg 3D chromatin architecture is established during their lineage specification, how it influences gene expression in Tregs, and whether and how Foxp3 contributes to Treg-specific chromatin interactions. Considering it was reported that Foxp3 has the capability to bring two distal DNA elements together through the formation a domain-swapped dimer[28], it would be of great interest to test whether that Foxp3 can function as a loop anchor protein to directly contribute to the establishment of Treg-specific TADs and chromatin loops.

Here, we comprehensively mapped the chromatin interactions across different Treg developmental stages in the thymus, and Treg and Tcon cells in the spleen by in situ Hi-C. Our findings revealed that the 3D genome of Treg cells is gradually established during Treg cell development, and Treg-specific chromatin interactions were associated with Treg signature gene expression. Furthermore, through comparison of WT Treg cells with “wannabe” Treg cells (isolated from Foxp3-GFP knock-in/knockout mouse), and Foxp3 domain-swap mutant (DSM) Treg cells (isolated from a newly-generated Foxp3 DSM mouse strain), our data showed that Foxp3 was critical for the establishment of Treg-specific chromatin interactions, although not likely dependent on the Foxp3 domain-swapped dimer to form Foxp3-associated chromatin loops. Our results revealed a previously unappreciated aspect of Foxp3 function in the regulation of Treg cell development and function.

RESULTS

Global transformation of 3D genome architecture during Treg lineage specification

To map the trajectory of the 3D genome organization during Treg lineage development, we performed *in situ* Hi-C experiments with T cells in different developmental stages, including $CD4^{-}CD8^{-}$ (DN), $CD4^{+}CD8^{+}$ (DP), $CD4^{-}CD8^{+}$ (CD8SP), $CD4^{+}CD8^{-}Foxp3^{-}CD25^{-}$ (CD4SP), $CD4^{+}CD8^{-}Foxp3^{-}CD25^{+}$ ($CD25^{+}$ Treg precursor), $CD4^{+}CD8^{-}Foxp3^{lo}CD25^{-}$ ($Foxp3^{lo}$ Treg precursor), $CD4^{+}CD8^{-}Foxp3^{+}CD25^{+}$ (Treg) from the thymus, and $CD4^{+}Foxp3^{-}$ (conventional T cells, Tcon) and $CD4^{+}Foxp3^{+}$ (mature Treg) from the spleen (Figure 1A and Supplementary Fig. 1). Chromatin interaction maps were constructed from Hi-C data at different resolutions down to 2kb resolution (Figure 1B). To examine patterns of gains and losses of chromatin interactions, we performed K-means clustering on normalized Hi-C contacts across each T cell population at 100kb resolution (Figure 1C). This revealed evidence for both gains and losses of chromatin interactions throughout the T cell developmental trajectory (Figure 1C,D). We next use T-distributed Stochastic Neighbor Embedding (t-SNE) map to visualize and compare different T cell subsets in two dimensions. t-SNE showed tight grouping between replicate experiments from the same T cell subset, indicating high reproducibility of the chromatin contact maps. Furthermore, the t-SNE map clearly showed a differentiation trajectory of Treg cell development in the thymus, in parallel to the trajectory generated based on gene expression profile of each T cell subset (Figure 1E). Therefore, the 3D genome structure is being reorganized following the differential steps of thymic Treg cell development.

Treg-specific chromatin contacts are associated with Treg gene expression and selective transcription factor binding activities.

108 To examine whether Treg cells have a unique 3D chromatin structure to support
109 their distinct gene expression profile and function, we performed a pairwise comparison
110 of the 3D chromatin structure of splenic Treg and Tcon cells. Using edgeR to detect
111 differential chromatin contacts at 25 kB resolution, we identified 1959 upregulated DNA
112 interactions in Treg cells and 1973 upregulated DNA interactions in Tcon cells (Figure
113 2A). As an example, we observed strong DNA interactions close to the *Socs2* gene locus
114 in Treg cells, but not in conventional T cells (Figure 1B). The Hi-C data showed that a
115 vast majority of DNA interactions were similar between Treg and Tcon, with only 0.29%
116 of tested chromatin interactions showing a significant change between Treg and Tcon
117 cells (3932/1377570). This small percentage agreed with previous studies showing that
118 less than 5% of the genes are differentially expressed in these two T cell
119 populations[19,29,30]. Additionally, Treg and Tcon cells share 99% of their enhancers, less
120 than 1% of the enhancers are unique to either T cell population[26].
121 We next examined whether the differences in 3-D chromatin structures between
122 Treg and Tcon cells are associated with changes in gene expression. Analysis of gene
123 expression profiles of Treg and Tcon cells revealed that 928 genes (FDR > 1% and Fold
124 change > 2) were differentially expressed (Figure 2C). Based on Hi-C data, of the 3932
125 differential chromatin interactions between Treg and Tcon cells, 617 chromatin interaction
126 anchors overlapped with the transcription start site of at least one gene. Strikingly, ~35%
127 of these anchors contained differentially expressed genes (216 of 617), which accounted
128 for about one-quarter of all differentially expressed genes (216 of 928) (Figure 1D). This
129 result suggested that differences in gene expression are potentially associated with
130 unique DNA interacting activities in Treg cells.

To further explore the link between chromatin interactions and gene expression, we determined the number of differential interacting partners for each individual interaction anchor that is proximal to a differentially expressed gene. While most loci with differential interactions had only one partner anchor, a minority of loci form multiple differential long-range contacts (Figure 2E). We observed that the loci with higher numbers of differential long-range interactions were more likely to be associated with differentially expressed genes (Figure 2F and 2G). Of note, the loci with more than 4 differential DNA interactions were associated with several well-established Treg signature genes, including *Ikzf2*, *Lrrc32* (encoding GARP), *Socs2*, and *Ptger4* (Figure 2G and 2H). These results further illustrated the correlation between changes in DNA interactions and differential gene expression in Treg cells.

To search for factors involved in establishing a Treg-specific 3D chromatin structure, we compared the relative enrichment of several transcription factors and chromatin structure regulators in Treg- and Tcon- specific loop anchors. Although CTCF and cohesin are critical for the formation of DNA loops[31,32], their relative enrichments in Tcon or Treg-specific loop anchors were moderate (Figure 2I). In contrast, multiple transcription factors, including Foxp3, Satb1, Runx1, Ets1, and Bcl11b, which are involved in Treg differentiation and function, showed a more pronounced enrichment in Tcon or Treg-specific interactions. Strikingly, the enrichment of Foxp3 bound peaks was ranked first among all the transcription factors tested, suggesting that Foxp3 might play a crucial role in Treg-specific loop formation (Figure 2I).

Foxp3 is critical for the establishment of Treg-specific 3D chromatin structure

154 Foxp3 is a pivotal regulator of Treg differentiation and function. Given that Foxp3
155 bound peaks are highly enriched in the anchor regions of Treg-specific chromatin
156 interactions, we examined Foxp3's role in the formation and maintenance of Treg-specific
157 DNA loops. To this end, we used a GFP knock-in Foxp3 knockout mouse strain
158 ($Foxp3^{GFP\text{-}KIKO}$)[30], in which GFP expression replaces Foxp3 and can be used as a
159 fluorescent marker to identify Treg "wannabe" cells (Figure 3A). Hi-C experiments were
160 performed with $GFP^{+}Foxp3^{-}$ Treg- "wannabe" cells from $Foxp3^{GFP\text{-}KIKO}$ mice and control
161 $GFP^{+}Foxp3^{+}$ WT Treg cells from $Foxp3^{GFP}$ mice. We focused on chromatin contacts that
162 were Treg specific in our comparison of Treg and Tcon chromatin interactions.
163 Comparison between the chromatin contacts in $GFP^{+}Foxp3^{+}$ WT Treg cells and
164 $GFP^{+}Foxp3^{-}$ Treg "wannabe" cells showed that a total of 124 out of 1569 Treg-specific
165 interactions were significantly reduced in the GFP^{+} Foxp3-KIKO cells (Figure 3B,
166 FDR=10%). While this represents a minority of the Treg-specific contacts (7.9% or
167 124/1569), the decrease in Treg-specific DNA contacts in Foxp3 KIKO cells was also
168 illustrated by the overall distributions of KIKO vs. WT contact frequency fold-changes
169 (Figure 3C). Specifically, 77.7% (1219/1569) of Treg-specific contacts showed a
170 decrease (fold change < 0) in chromatin interaction frequency in GFP^{+} Foxp3-KIKO cells
171 relative to control $GFP^{+}Foxp3^{+}$ WT Treg cells. The reduction of chromatin interactions in
172 $GFP^{+}Foxp3^{-}$ Treg- "wannabe" cells could be seen at the locus of the Ikzf2 gene, one of
173 the Treg signature genes. In Tcon cells, there were no detectable chromatin interactions
174 around Ikzf2, while strong DNA interacting loops emerged in WT Treg cells. In the Treg-
175 "wannabe" cells, the chromatin interactions were significantly weakened at the Ikzf2 locus
176 (Figure 3D). ChIP-seq and Cut&Run experiments showed the DNA looping anchors

around *Ikzf2* were enriched with Foxp3 bound peaks along with CTCF and cohesin component Smc1a bound peaks (Figure 3E). The fact that some but not all Treg specific chromatin interactions lost in GFP^{+}Foxp3^{-} Treg- “wannabe” cells led us to investigate whether contacts lost in GFP^{+}Foxp3^{-} Treg- “wannabe” cells may be more dependent on Foxp3. Indeed, chromatin contacts that were lost in the Treg- “wannabe” cells compared to controls were more likely to contain Foxp3 binding peaks (Figure 3F). In addition to Foxp3 binding sites, we also examined the enrichment of transcription factor (TF) motifs in Treg DNase I Hypersensitive Sites (DHS), and identified motifs with differential TF motif enrichment in chromatin contacts lost versus retained in GFP^{+}Foxp3^{-} Treg- “wannabe” cells versus control cells (Figure 3G). Specifically, we saw modest enrichments of CTCF, ETS-family, and MEF2B/D TF motifs in DHS sites at chromatin contacts retained in GFP^{+}Foxp3^{-} Treg- “wannabe” cells. This suggests that these TFs, in conjunction with Foxp3, may be critical for the establishment of the mature Treg 3D chromatin landscape. Taken together, these data suggest that the establishment of Treg-specific chromatin interactions is dependent on Foxp3 expression.

Mutations in the Foxp3 domain-swapped dimerization interface lead to inadvertent immune system activation in mice.

Although our data clearly indicated that Foxp3 is indispensable for establishing Treg-specific 3D chromatin structure, it is not clear whether Foxp3 is directly involved in DNA looping like CTCF/cohesin, or whether it acts indirectly as a factor that facilitates the binding of architectural proteins including CTCF and cohesin to form Treg-specific chromatin interactions. It was reported that Foxp3 is able to form a domain-swap (DS)

200 dimer through its forkhead domain to bring two distal DNA elements together[28],
201 suggesting Foxp3 has the potential to facilitate DNA looping directly (Figure 4A). To test
202 this possibility, we generated a Foxp3 domain-swapped mutant (DSM) mouse strain by
203 using the CRISPR technology. Three amino acid mutations (W348Q, M370T and A372P)
204 were introduced to the Foxp3 coding region in the Foxp3-IRES-Thy1.1 reporter mouse
205 (Figure 4B). After verifying the mutations by DNA sequencing, we analyzed Foxp3 DSM
206 mice and WT littermate controls to determine whether disabling Foxp3's domain swapped
207 dimerization affects Treg cell development and function. The Foxp3 DSM mice appeared
208 to be normal up to 2 months of age when they started to develop a moderate
209 lymphoproliferative disease with loss of body weight and increased cellularity in the
210 spleen (Figure 4C, D). The frequency of Treg cells was higher while Foxp3 protein level
211 was significantly reduced in Foxp3 DSM mice compared to WT controls (Figure 4E).
212 CD4+ conventional T cells and CD8+ T cells were also more activated with the expansion
213 of the CD44+CD62L^{low} population. (Figure 4F). Consistently, IFNγ production increased
214 significantly in splenic CD4+ T cells from Foxp3 DSM mouse (Figure 4G). Furthermore,
215 serum concentrations of IgG1 and IgM were significantly higher in Foxp3 DSM mice
216 compared to WT controls (Figure 4H). Histopathology analysis of 6- to 9-month-old Foxp3
217 DSM mice revealed widespread immune cell infiltration in the lung, liver, small intestine,
218 and salivary gland tissues (Figure 4I). Taken together, these data suggested that the
219 inability of Foxp3 to dimerize in "trans" leads to a moderate defect in Treg cell's immune
220 suppressive function which results in excessive immune system activation.
221

The formation of Treg-specific chromatin interactions is independent of Foxp3 domain-swap dimerization

Next, we sought to assess whether the impairment of Foxp3 DSM Treg function was because domain-swap mutation disrupted the formation of Treg 3D genome structure, and subsequently affected Treg signature gene expression. To this end, we isolated Treg cells from 6-week-old asymptomatic Foxp3 DSM and control mice and performed in-situ Hi-C experiments to map their 3-D genome structure. Foxp3 DSM and WT Treg cells showed similar chromatin interaction patterns as a whole and within Treg-specific interactions (Figure 5A). In fact, none of the 1445 Treg specific chromatin interactions is significantly different in the DSM Tregs compared to the WT Tregs (FDR<10%) (Figure 5B). Furthermore, we did not observe a global loss of chromatin contacts at Treg-specific interactions in the DSM Treg cells as we do in the GFP^{+} Foxp3 KIKO cells (Figure 5C). Finally, the lack of differences in 3D structure between DSM and WT Tregs was not related to statistical power or data quality, as the sequencing depth and Hi-C library quality was comparable between Tcon, Treg, KIKO, and DSM experiments (Supplementary Table 1). Taken together, these results show that domain-swapped dimerization of Foxp3 is not required for establishing Treg-specific 3-D genome structure.

To further dissect the molecular mechanism underlying DSM Treg's impaired function, we performed RNA-seq experiments with DSM and WT Treg cells. There were 26 up-regulated genes and 121 down-regulated genes in DSM Tregs compared to WT Tregs (Figure 5D, FDR 5%, greater than 2-fold change). Interestingly, the differentially expressed genes in the DSM Treg cells showed expression patterns resembling naïve T cells, rather than WT Treg cells (Figure 5E), suggesting that the domain-swap mutation

disrupts Foxp3's transcriptional regulation function of Foxp3. The expression of several Treg signature genes, *Lrrc32* (encodes the GARP protein), *Tigit*, and *Ctla4*, were compromised in DSM Tregs, contributing to their impaired immune suppressive function.

To further explore the mechanism underlying dysregulated gene expression in DSM Tregs despite the lack of changes in 3D genome structure, we examined whether the DSM mutation contributed to differences in Foxp3 binding using CUT&RUN. We identified 36,727 Foxp3 binding peaks in WT and DSM Tregs by CUT&RUN. Comparing peak strength between WT and DSM-mutant Tregs, we identified 295 peaks that showed differential Foxp3 binding (Figure 5F, FDR 5%). We then analyzed differential Foxp3 binding peaks based on their distance to differentially expressed genes in WT and DSM Tregs. The differential DSM Foxp3 binding peaks were significantly closer to DEGs compared to non-affect Foxp3 binding peak controls (Figure 5G). For example, although chromatin interactions around *Lrrc32* were similar, the main Foxp3-bound peak was weaker in DSM Tregs compared to WT controls (Figure 5H, 5I). It is likely that defective Foxp3 binding resulted in the reduced expression level of Lrcc32 in DSM Tregs (Figure 5J). Taken together, these results suggest that the domain-swapped mutation negatively affects Foxp3 binding to the loci of a subset of genes, leading to compromised gene expression and defective Treg function.

Foxp3-associated chromatin interactions are functionally required for Treg cell function

To further understand how Foxp3 is involved in the establishment of Treg-specific chromatin interaction, we performed proximity ligation-assisted ChIP-seq (PLAC-seq)[33]

268 with an antibody against Foxp3 in Treg cells, which enabled us to analyze Foxp3-
269 associated chromatin interactions with higher sensitivity and efficiency. Using Foxp3
270 PLAC-seq data, we identified focal loops at 10 kB resolution. These focal loops were
271 highly overlapped with Foxp3 binding peaks in Treg cells (Figure 6A). In total, we
272 identified 2169 Foxp3-associated loop anchors, of which the majority contained a Foxp3
273 binding site or had a Foxp3 binding site within 10 kB (Figure 6B). Of note, 9.01% of the
274 total Foxp3 binding sites are associated with chromatin interactions identified by Foxp3
275 PLAC-seq (Figure 6C). We next classified Foxp3-associated DNA loops based on the
276 locations of the loop anchors relative to genes. More than two-thirds of the loops are
277 gene-gene (22.49% vs. expected 4.35%), gene-enhancer (27.12% vs expected 2.61%),
278 enhancer-enhancer (17.17% vs. expected 1.14%) interactions, implicating their
279 involvement in the regulation of gene expression (Figure 6D).

280 To examine how Foxp3-associated chromatin interactions influence gene
281 expression, we compared the expression of genes whose transcription starting site
282 overlaps with Foxp3 PLAC-seq interactions between CD4+ conventional T cells and
283 Tregs. A number of Treg signature genes, including Ikzf2, Icos, Entpd1, and Il7r, emerged
284 as associated with Foxp3 PLAC-seq interactions (Figure 6E). We next directly tested
285 whether Foxp3-associated chromatin loops facilitate gene expression at the Ikzf2 locus.
286 Using a pair-guide RNA mediated CRISPR/Cas9 approach[34], we systemically deleted 9
287 Foxp3 binding sites (named P1 to P9) located close to the Ikzf2 gene, and measured
288 Helios protein (encoded by the Ikzf2 gene) expression in Treg cells compared to cells
289 transduced with non-targeting sgRNAs (Figure 6F and Supplementary Fig. 2). When the
290 Foxp3 binding site at the P1 or P6 regions were deleted, Helios expression decreased

291 significantly (Figure 6G). The P6 region is located in the Ikzf2 promoter, therefore its
292 deletion served as a positive control. We next deleted the P1 or P6 region in mature
293 splenic Treg cells in vitro, which were then transferred into Rag1 knockout recipient mice
294 to track deletion's impact on Tregs *in vivo*. Indeed, Helios expression was reduced in
295 Tregs isolated from P1 deleted Treg cells (Figure 6H), suggesting that the P1 region is a
296 Foxp3 bound enhancer. Interestingly, Hi-C analysis showed that P1 deletion did not
297 significantly weaken Foxp3 PLAC-seq peak at the Ikzf2 locus (Figure 6I). This data
298 suggests that Foxp3 may not be required for the maintenance of Treg-specific chromatin
299 interactions, despite that Foxp3 binding is essential for Ikzf2 expression.

300 To further characterize Foxp3's role in the maintenance of Treg-specific chromatin
301 interactions in mature Treg cells, we used CRISPR/Cas9 to knockout Foxp3 in splenic
302 Treg cells *in vitro*, and profiled their 3D genome structure by in situ Hi-C (Supplementary
303 Fig. 3A, B). Unlike $GFP^{+}Foxp3^{-}$ KIKO cells, the deletion of Foxp3 by sgRNA in mature
304 Treg cells did not change their chromatin interaction patterns as a whole or within Treg-
305 specific interactions (Supplementary Fig. 3C). There was no global loss of chromatin
306 contacts at Treg-specific interactions in the sgFoxp3 Treg cells as in the GFP^{+} $Foxp3^{-}$
307 KIKO cells (Supplementary Fig. 3D). Therefore, Foxp3 is essential for establishing Treg-
308 specific chromatin interactions but dispensable for the maintenance of these interactions
309 in mature Treg cells.

310 To further investigate Foxp3's role in Treg gene expression, we compared Treg-
311 specific genes, which are differentially expressed between Treg and Tcon cells, with
312 genes that are dysregulated in either the KIKO or DSM Treg cells. This divided the Treg-
313 specific genes into two sets, "Foxp3 dependent" (changing in KIKO or DSM or both) and

Foxp3 independent (not changing in KIKO or DSM) (Figure 7A). Gene Ontology (GO) analysis of these two sets of genes revealed distinct GO terms. For the Foxp3-dependent genes, the top terms were related to immune function, cytokines, and cell adhesion (Figure 7B). For the Foxp3 independent genes, the top hits were related to metabolism and cell cycle (Figure 7C). This was not caused by a specific p-value threshold, because by comparing the GO terms obs/exp gene sets, there were a large number of GO terms that were specific to the Foxp3 dependent or independent set (Figure 7D). Furthermore, about 3/4 of all the GO terms that came up as significant in either the foxp3 dependent or independent sets are specific to each set (Figure 7E). These analyses suggested that Foxp3 regulates genes related to the immune function of Treg cells, while other factors regulate cell cycle and cell metabolic processes during Treg lineage commitment.

DISCUSSION

In this study, we examined the role of Treg lineage-specific transcription factors Foxp3 in 3D genome organization during the late stage of T cell development. We compared the 3D chromatin structures of Treg cells and their precursors and revealed that the 3D chromatin architecture of Treg cells was gradually established during Treg lineage specification, and that changes in chromatin interactions align with the trajectory of Treg development. By comparing Treg cells and their closely related conventional T cells, we identified chromatin structures unique to Treg cells. Overall, the Treg's chromatin structure was highly similar to that of conventional T cells, 0.29% (3932/1377570) chromatin interactions were significantly different between Treg and Tcon cells. This small number of differential chromatin interactions are in line with less

337 than 1% of differential enhancers, and less than 5% of differentially expressed genes
338 between Treg and conventional T cells. Strikingly, these Treg-specific chromatin
339 interactions were frequently associated with the loci of Treg signature genes.

340 Our study investigated Foxp3's contribution to the establishment and maintenance
341 of Treg's chromatin structure. Notably, Foxp3 was significantly enriched at the anchor
342 regions of Treg-specific chromatin loops, even ranking higher than CTCF/cohesin. By
343 taking advantage of Treg-"wannabe" cells from Foxp3$^{GFP\text{-}KIKO}$ mice, our data revealed that
344 Foxp3 was essential for the establishment of Treg-specific chromatin structure, which
345 agreed with a recently published Foxp3 HiChIP study[27]. It was proposed that the domain-
346 swapped dimer of Foxp3 facilitates its potential role as a DNA loop anchor to establish
347 Treg-specific chromatin interactions[28]. We further examined whether Foxp3 can function
348 as a DNA loop anchor by comparing of WT and DSM Treg cells. Although the Foxp3 DSM
349 Treg cells were dysfunctional and the Foxp3 DSM mice developed lymphoproliferative
350 disease, the 3D chromatin architecture of the Treg cells was not affected by mutations
351 disrupting Foxp3 domain-swapped dimerization. Instead, the defective function of DSM
352 Tregs is likely caused by impaired Foxp3 binding to key Treg gene loci. Furthermore, a
353 recent study showed that the Foxp3 domain-swapped dimer is dysfunctional, while a
354 head-to-head dimer represents the physiological form of Foxp3[35]. Altogether, these data
355 suggested that domain-swapped dimerization of Foxp3 is not required for the organization
356 of Treg's 3D chromatin structure.

357 The Foxp3 PLAC-seq and Foxp3 ChIP-seq/CUT&RUN data also revealed that
358 Foxp3-associated chromatin interactions were associated with the loci of Treg-signature
359 genes, including *Ikzf2*, *Icos*, *Entpd1*, and *Il7r*. Although the deletion of Foxp3 binding sites

360 in the Ikzf2 locus decreased its expression, it did not disrupt the chromatin interactions at
361 the corresponding regions. Furthermore, the ablation of Foxp3 in mature Treg cells did
362 not alter their 3D genome structure. This data indicates that although Foxp3 plays an
363 essential role in the formation of Treg-specific chromatin interactions, it is not required for
364 their maintenance of the Treg's 3D chromatin structure. Furthermore, by comparing WT
365 Treg, "wannabe" Treg, and DSM Treg gene expression, we found that Treg-characteristic
366 genes can be separated into Foxp3-dependent and Foxp3-independent groups, with
367 Foxp3-dependent genes enriched in Treg immune suppressive functions, while Foxp3-
368 independent genes enriched in metabolic and cell cycle regulations.

369 In summary, our data suggest that Foxp3 as a Treg lineage-specific transcription
370 factor facilitates chromatin structure reorganization to establish Treg's cell identify. Since
371 Foxp3 by itself does not function as a chromatin loop anchor to stabilize chromatin
372 interactions, it likely cooperates with other proteins such as CTCF, cohesin, and YY1[36] to
373 set up Treg-specific 3D genome structure during Treg development. Once the 3D genome
374 structure is formed in mature Tregs, Foxp3 is not required for its maintenance. Instead,
375 Foxp3 acts as a transcription factor to activate or repress gene expression by leveraging
376 the promoter-enhancer proximity facilitated by the Treg-specific chromatin looping
377 structure. This study presented a model of how lineage-specific transcription factors
378 function during the late or terminal stage of cell differentiation.
379

Acknowledgments

We would like to thank T. Hua, N. Tessler, and C. Gordon for mouse colony management, C. O'Connor for assistance in flow cytometry, Y. Dayn for assistance in generating the Foxp3 DSM mutant mice. Z.L. was supported by a NOMIS Fellowship. D.S.L. was supported by the 2022 Advanced Facility Fund of the University of Seoul. Y.Z. was supported by the NOMIS Foundation, the Crohn's and Colitis Foundation, the Sol Goldman Trust, and National Institutes of Health (R01-AI107027, R01-AI1511123, R21-AI154919, and S10-OD023689). J.R.D. was supported by National Institutes of Health (DP5-OD023071 and U01-CA260700). This work was also supported by National Cancer Institute funded Salk Institute Cancer Center Core Facilities (P30-CA014195).

Author Contributions

Conceptualization: Z.L., D.L., Y.Z., and J.R.D. Methodology: Z.L. and D.L. Investigation: Z.L., D.L., and Y.L. Resources: Y.Z. and J.R.D. Formal analysis: Z.L., D.L., and J.R.D. Data Curation: Z.L. D.L., and J.R.D. Supervision: Y.Z. and J.R.D. Funding acquisition: Y.Z. and J.R.D Writing – original draft preparation: Z.L., D.L., Y.Z., and J.R.D. Writing – review and editing: Z.L., D.L., Y.Z., and J.R.D.

Figure Legends

Figure 1. Chromatin architecture reorganization during T cell lineage commitment. A) Schematic of experimental design to study changes in chromatin architecture during T cell lineage commitment. B) Example Hi-C heat maps in mature splenic Treg cells at progressively higher resolutions near the Bcl11b gene. C) Clustering of chromatin interactions in thymic T cell subsets. Chromatin interactions were calculated at a resolution of 100kb and clustered using K-means clustering (K=10). Replicate experiments were also clustered using hierarchical clustering. D) Hi-C chromatin interactions over specific loci that gain or lose chromatin contacts during T cell lineage commitment. E) T-distributed stochastic neighbor embedding (tSNE) of chromatin contacts (left panel) and gene expression (right panel) during T cell lineage commitment.

Figure 2. Chromatin conformation changes between Treg cells and conventional CD4+ T cells. A) Chromatin interaction frequency of 25kb bins compared between conventional CD4+ T cells (x-axis) and Treg cells (y-axis). Interactions called as differential between Treg and Tcon cells are labelled red (FDR 1%). B) Hi-C browser shot of a region showing Treg specific interactions. The Hi-C plot shows interactions over a ~800kb locus containing a cluster of Treg upregulated genes (Plxnc1, Socs2, Ube2n, Nudt4). Below the Hi-C data is a genome browser track of ChIP-seq for CTCF (green), Smc1a (purple), H3K27ac (blue), and Foxp3 (orange, showing ChIP-seq and Cut&Run) in Treg and Tcon cells. C) Plot of transcript abundance (x-axis) versus fold change (y-axis) of gene expression between CD4+ Tcon cells and Treg cells. Points show in red are called as differentially expressed genes (FDR 1%, minimum 2-fold change). D) Venn

diagram showing overlap between regions of the genome showing differential chromatin contacts (purple) and the transcription start site of genes showing Treg specific expression (green) (p-value by Fisher's exact test). E) Histogram of the number of differential interacting partners for each differential interaction anchor. Most loci are involved in differential interactions with one partner anchor, but a minority of loci form multiple differential long-range contacts. F) Fraction of anchors of differential chromatin interactions that overlap differentially expressed genes for loci involved in one or more differential interactions. Loci involved with multiple differential long-range interactions are more likely to contact differentially expressed genes. G) Heat map of genes overlapping anchors involved in >4 differential chromatin interactions (log2 fold-change). H) Example of multi-way long-range differential chromatin interaction. Treg chromatin interactions are shown in the upper right hand portion of the heat map, and Tcon chromatin interactions are shown in the lower left hand portion of the heat map. I) Enrichment of ChIP-seq peaks over differential chromatin interactions. ChIP-seq data is shown either from CD4+ Tcon cells (pink box) or Treg cells (blue box). Enrichment is shown for Tcon specific interactions (yellow bars) or Treg specific interactions (blue bars).

Figure 3. Foxp3 is required for the complete establishment of Treg specific 3D chromatin structure. A) Schematic of the Foxp3-GFP knock-in and the Foxp3-GFP (WT) and Foxp3 knock-in/knock-out (KIKO) mice. eGFP is knocked into the Foxp3 locus in both the Foxp3-GFP and KIKO mice. In KIKO mouse, the eGFP is followed by 3x stop codons to prevent Foxp3 protein translation. B) Chromatin interaction frequency between WT and KIKO Treg cells at N=1569 Treg specific chromatin interactions. Treg specific chromatin

interactions were identified by comparison of splenic Treg and Tcon cells as shown in Figure 2. Differential chromatin interactions (N=125/1569) are labeled as points in red (FDR = 10%). C) Violin plot of the log2 fold-change in interaction frequency between Foxp3 WT and KIKO Treg cells at Treg specific chromatin interactions. The median log2 fold change is -0.24 (black dot) consistent with a loss of chromatin interactions in KIKO Tregs at Treg specific chromatin interactions. D) Hi-C interaction maps at the Ikzf2/Helios gene in Tcon, Treg, Foxp3 WT Treg, and Foxp3 KIKO Tregs (left to right). E) Chromatin interactions in Treg cells at the Ikzf2/Helios locus and the associated ChIP-seq or CUT&RUN experiments over the locus. F) Enrichment of Foxp3 CUT&RUN peaks over Treg specific chromatin interactions that are either retained in KIKO cells (gray) or lost in KIKO cells (blue) showing that the regions that lose chromatin interactions in Foxp3 KIKO cells are more likely to have Foxp3 binding sites. G) Observed vs. expected motif frequency in DNase I Hypersensitive sites overlapping chromatin interactions lost in Foxp3 KIKO cells (x-axis) vs. chromatin interactions retained in Foxp3 KIKO cells (y-axis).

Figure 4. Foxp3 domain swap mutant mice develop an autoinflammatory phenotype. A) Schematic of Foxp3 domain swap dimer. Two Foxp3 proteins interact as a dimer (white and pink chains) binding to two DNA strands in a “trans” configuration. Structure from PDB accession 3QRF. B) Strategy for generation of Foxp3 domain swap mutant mice by CRISPR/Cas9. Two sgRNAs were used to cut off the endogenous genomic fragment, and a synthesized single-strand DNA with domain swap mutation was used to guide CRISPR/Cas9 mediated homology-directed repair. C-I) 6- to 9-month-old Foxp3 DSM (n=13) and WT (n=5) littermate control mice were analyzed for C) Body

weight, D) spleen cellularity, E) Frequency of Foxp3+ Treg cells in total CD4+ T cells and Foxp3 protein level. F) frequency of $CD44^{+}CD62l^{lo}$ cells in CD4+ Tcon and CD8+ T cells, G) frequency of $IFN\gamma^{+}$ and $IL\text{-}17^{+}$ cells in CD4+ Tcon cells. H) ELISA quantification of the concentrations of IgG1, IgM, IgG2c, and IgA in serum. I) Representative hematoxylin and eosin staining of small intestine, liver, kidney, and lung sections from WT and Foxp3 DSM mice.

Figure 5. Foxp3 domain swap mutant and its impact on 3D genome structure and gene expression. A) Hi-C chromatin interactions in wild-type (WT) Treg cells (x-axis) and Foxp3 domain swap mutant (DSM) Treg cells (y-axis). Treg specific interactions between Treg and Tcon cells are labeled in red. B) Plot of chromatin interaction frequency (x-axis) versus log2 fold change in chromatin interaction frequency (y-axis) between DSM and WT Treg cells. Points shown in red are called as significant differential interactions (FDR 10%). C) Violin plot of the log2 of the fold change in interaction frequency between Foxp3 WT and Foxp3 KIKO Treg cells (red) or between Foxp3 WT and Foxp3 DSM Treg cells (green) over Treg specific chromatin interactions. The black dots show the median fold-change. D) Volcano plot of RNA-seq expression data between DSM and WT Treg cells. The x-axis shows log2 fold change in expression, while the y-axis shows -1*log10(p-value). Points labeled in red are genes that are significantly differentially expressed between DSM and WT Tregs (FDR 1%, 2 fold minimum change). E) Heat map of expression in CD4+ Tcon cells and different WT or DSM mutant Treg cells over genes differentially expressed between CD4+ Tcon cells and Treg cells. F) Foxp3 CUT&RUN peak enrichment in Foxp3 WT Treg (x-axis) and Foxp3 DSM Treg (y-axis) cells. Points in

red (N=295) show significantly differential Foxp3 peaks (FDR 5%). G) Cumulative density plot of the distance between differential Foxp3 peaks and differentially expressed genes (purple) compared to the distance between all Foxp3 peaks and differentially expressed genes (gray) showing that Foxp3 peaks affected by the DSM mutation are closer to DSM dysregulated genes (p-value is calculated by Wilcoxan test). H) Chromatin interactions near the Lrrc32 gene in Foxp3 WT Treg cells (upper right) versus Foxp3 DSM Treg cells (lower left). The dashed line box shows a distal enhancer with a Foxp3 peak with reduced binding in DSM Treg cells. I) Enhancer in the dashed box from panel H showing the reduction in Foxp3 binding in DSM Treg cells by Foxp3 CUT&RUN. J) Expression of Lrrc32 in Tcon, Treg, Foxp3 WT Treg, and Foxp3 DSM Treg cells showing reduced Lrrc32 expression in DSM Treg cells.

Figure 6. Foxp3-associated chromatin interactions link distal enhancers to Treg signature genes. A) Chromatin contact map of Foxp3 PLAC-seq data near the T reg specific genes Tnfaip3 and Ifngr1. Shown below the map are genome browser tracks of H3K27ac ChIP-seq (blue) and Foxp3 CUT&RUN (orange). B) Pie chart showing the fraction of Foxp3 PLAC-seq anchors that contain a Foxp3 binding site (yellow), are within 10kb of a Foxp3 binding site (+/- 1 bin, tan), or do not overlap with Foxp3 binding site (grey). C) Plot showing the fraction of Foxp3 binding sites associated with PLAC-seq interactions. The observed overlap (9.01%) is shown as a dashed line, while the distribution of random overlaps (1000 iterations) is shown in grey. D) Pie chart showing the fraction of Foxp3 PLAC-seq peaks that link genes (Gene), enhancers (Enh), or unannotated regions (Un). Enhancers are defined as distal H3K27ac peaks. Unannotated

regions are sites that do not overlap gene transcription start sites or distal H3K27ac peaks. E) Gene expression in CD4+ Tcon cells (x-axis) and Treg cells (y-axis) of genes whose TSS overlaps with Foxp3 PLAC-seq interactions. Points shown in red are genes called as differentially expressed between Treg and Tcon cells (FDR1%, 2-fold minimum change). F) Foxp3 PLAC-seq data near the Ikzf2/Helios locus. Shown below the interaction map are ChIP-seq and CUT&RUN tracks at the locus as well as the locations of Foxp3 binding sites targeted for CRISPR deletion across the locus (P1-P9). G) The effect of CRISPR deletion of Foxp3 binding sites P1 or P6 on Helios expression in Treg cells in vitro. H) In vivo validation of the effect of P1 or P6 deletion on Helios expression. Treg cells transduced with gRNAs targeting P1 or P6 were co-transferred with Tregs with control gRNAs into the same Rag1-/- mice, and Helios expression was then analyzed 2 weeks post transfer. I) Hi-C interaction map at the Ikzf2/Helios gene in Treg cells transduced with control gRNAs (upper right) or gRNAs targeting P1 (lower left).

Figure 7. Foxp3 dependence defines differential programs of Treg lineage commitment. A) Gene expression of genes differentially expressed between Tcon and Treg cells across Foxp3 WT and mutant cells. Genes are separated into those that show significant differences in the Foxp3 KIKO, DSM, or both mutants (“Foxp3 dependent”) and those that show differential regulation in Tcon vs. Treg cells but do not show differences in the Foxp3 mutant cells (“Foxp3 independent”). B) Gene ontology analysis of the “Foxp3 dependent” genes shows terms related to immune differentiation and function. C) Gene ontology analysis of “Foxp3 independent” genes shows terms related to metabolic regulation and the cell cycle. D) Comparison of the observed/expected Gene ontology

537 term frequency for Foxp3 dependent (x-axis) versus independent (y-axis) genes shows
538 an inverse correlation of enrichment of ontology terms. E) Pie chart of gene ontology
539 terms that are significant for either “Foxp3 dependent” or “Foxp3 independent” genes that
540 are significant in both sets (purple) or Foxp3 independent alone (red) or Foxp3 dependent
541 alone (blue).
542

Supplementary Figure Legends

Supplementary Figure 1. Flow cytometry isolation of T cell populations in the thymus and spleen. A) Flow cytometric gating strategy to isolate T cells in the thymus, including $CD4^{-}CD8^{-}$ (DN), $CD4^{+}CD8^{+}$ (DP), $CD4^{-}CD8^{+}$ (CD8SP), $CD4^{+}CD8^{-}Foxp3^{-}CD25^{-}$ (CD4SP), $CD4^{+}CD8^{-}Foxp3^{-}CD25^{+}$ ($CD25^{+}$ Treg precursor), $CD4^{+}CD8^{-}Foxp3^{lo}CD25^{-}$ ($Foxp3^{lo}$ Treg precursor), $CD4^{+}CD8^{-}Foxp3^{+}CD25^{+}$ (Treg). B) Flow cytometric gating strategy to isolate $CD4^{+}Foxp3^{-}$ (conventional T cells, Tcon) and $CD4^{+}Foxp3^{+}$ (mature Treg) from the spleen.

Supplementary Figure 2. CRISPR deletion of Foxp3 sites near the Ikzf2 gene. A) Hi-C chromatin interactions near the Ikzf2 gene. The heatmap shows Hi-C data near Ikzf2, while the ChIP-seq tracks below show signals for CTCF and Foxp3 binding. Also labeled are the locations of the 9 deleted Foxp3 sites (P1-P9). B) Flow cytometric analysis of the expression of Helios after CRISPR knockout of indicated Foxp3-bound sites (Ikzf2 P1-P9) in Treg cells.

Supplementary Figure 3. CRISPR/Cas9 deletion of Foxp3 in mature Treg cells. A) Schematic of experimental strategy for deletion of Foxp3 in mature Treg cells. B) FACS plots showing sgFoxp3 targeting efficiency in knockdown of Foxp3 expression in Treg cells. C) Comparison of chromatin interactions between sgControl and sgFoxp3 targeted Treg cells. The plot shows the strength of chromatin contacts (X-axis) and the fold change in chromatin interaction frequency (y-axis) between sgControl and sgFoxp3 targeted cells. Only one interacting locus shows a significant difference in interaction frequency (colored

566 in red). D) Violin plots of fold change in chromatin interaction frequency between mutant
567 and wild type comparing the effects in the Foxp3 KIKO Treg cells (left, orange) and in
568 Foxp3 sgRNA targeted cells (right, blue).
569

References

1 Lieberman-Aiden, E. *et al.* Comprehensive mapping of long-range interactions reveals folding principles of the human genome. *Science* **326**, 289-293, doi:10.1126/science.1181369 (2009).

2 Rao, S. S. *et al.* A 3D map of the human genome at kilobase resolution reveals principles of chromatin looping. *Cell* **159**, 1665-1680, doi:10.1016/j.cell.2014.11.021 (2014).

3 Dixon, J. R. *et al.* Topological domains in mammalian genomes identified by analysis of chromatin interactions. *Nature* **485**, 376-380, doi:10.1038/nature11082 (2012).

4 Bonev, B. & Cavalli, G. Organization and function of the 3D genome. *Nat Rev Genet* **17**, 661-678, doi:10.1038/nrg.2016.112 (2016).

5 Schmitt, A. D., Hu, M. & Ren, B. Genome-wide mapping and analysis of chromosome architecture. *Nat Rev Mol Cell Biol* **17**, 743-755, doi:10.1038/nrm.2016.104 (2016).

6 Dixon, J. R., Gorkin, D. U. & Ren, B. Chromatin Domains: The Unit of Chromosome Organization. *Mol Cell* **62**, 668-680, doi:10.1016/j.molcel.2016.05.018 (2016).

7 Zheng, H. & Xie, W. The role of 3D genome organization in development and cell differentiation. *Nat Rev Mol Cell Biol* **20**, 535-550, doi:10.1038/s41580-019-0132-4 (2019).

8 Stadhouders, R., Filion, G. J. & Graf, T. Transcription factors and 3D genome conformation in cell-fate decisions. *Nature* **569**, 345-354, doi:10.1038/s41586-019-1182-7 (2019).

9 Merkenschlager, M. & Nora, E. P. CTCF and Cohesin in Genome Folding and Transcriptional Gene Regulation. *Annu Rev Genomics Hum Genet* **17**, 17-43, doi:10.1146/annurev-genom-083115-022339 (2016).

10 Johanson, T. M. *et al.* Transcription-factor-mediated supervision of global genome architecture maintains B cell identity. *Nat Immunol* **19**, 1257-1264, doi:10.1038/s41590-018-0234-8 (2018).

11 Kim, S. & Shendure, J. Mechanisms of Interplay between Transcription Factors and the 3D Genome. *Mol Cell* **76**, 306-319, doi:10.1016/j.molcel.2019.08.010 (2019).

12 Hu, G. *et al.* Transformation of Accessible Chromatin and 3D Nucleome Underlies Lineage Commitment of Early T Cells. *Immunity* **48**, 227-242 e228, doi:10.1016/j.immuni.2018.01.013 (2018).

13 Wang, W. *et al.* TCF-1 promotes chromatin interactions across topologically associating domains in T cell progenitors. *Nat Immunol* **23**, 1052-1062, doi:10.1038/s41590-022-01232-z (2022).

14 Shan, Q. *et al.* Tcf1-CTCF cooperativity shapes genomic architecture to promote CD8(+) T cell homeostasis. *Nat Immunol* **23**, 1222-1235, doi:10.1038/s41590-022-01263-6 (2022).

15 Sakaguchi, S. *et al.* Regulatory T Cells and Human Disease. *Annu Rev Immunol* **38**, 541-566, doi:10.1146/annurev-immunol-042718-041717 (2020).

16 Josefowicz, S. Z., Lu, L. F. & Rudensky, A. Y. Regulatory T cells: mechanisms of differentiation and function. *Annu Rev Immunol* **30**, 531-564, doi:10.1146/annurev.immunol.25.022106.141623 (2012).

612 17 Hori, S., Nomura, T. & Sakaguchi, S. Control of regulatory T cell development by the
613 transcription factor Foxp3. *Science* **299**, 1057-1061, doi:10.1126/science.1079490
614 (2003).
615 18 Fontenot, J. D., Gavin, M. A. & Rudensky, A. Y. Foxp3 programs the development and
616 function of CD4+CD25+ regulatory T cells. *Nat Immunol* **4**, 330-336, doi:10.1038/ni904
617 (2003).
618 19 Fontenot, J. D. *et al.* Regulatory T cell lineage specification by the forkhead transcription
619 factor foxp3. *Immunity* **22**, 329-341, doi:10.1016/j.immuni.2005.01.016 (2005).
620 20 Williams, L. M. & Rudensky, A. Y. Maintenance of the Foxp3-dependent developmental
621 program in mature regulatory T cells requires continued expression of Foxp3. *Nat*
622 *Immunol* **8**, 277-284, doi:10.1038/ni1437 (2007).
623 21 Kwon, H. K., Chen, H. M., Mathis, D. & Benoist, C. Different molecular complexes that
624 mediate transcriptional induction and repression by FoxP3. *Nat Immunol*,
625 doi:10.1038/ni.3835 (2017).
626 22 Angelin, A. *et al.* Foxp3 Reprograms T Cell Metabolism to Function in Low-Glucose, High-
627 Lactate Environments. *Cell Metab*, doi:10.1016/j.cmet.2016.12.018 (2017).
628 23 Zheng, Y. & Rudensky, A. Y. Foxp3 in control of the regulatory T cell lineage. *Nat*
629 *Immunol* **8**, 457-462, doi:10.1038/ni1455 (2007).
630 24 Van Gool, F. *et al.* A Mutation in the Transcription Factor Foxp3 Drives T Helper 2
631 Effector Function in Regulatory T Cells. *Immunity* **50**, 362-377 e366,
632 doi:10.1016/j.immuni.2018.12.016 (2019).
633 25 Rudra, D. *et al.* Transcription factor Foxp3 and its protein partners form a complex
634 regulatory network. *Nat Immunol* **13**, 1010-1019, doi:10.1038/ni.2402 (2012).
635 26 Samstein, R. M. *et al.* Foxp3 exploits a pre-existent enhancer landscape for regulatory T
636 cell lineage specification. *Cell* **151**, 153-166, doi:10.1016/j.cell.2012.06.053 (2012).
637 27 Ramirez, R. N., Chowdhary, K., Leon, J., Mathis, D. & Benoist, C. FoxP3 associates with
638 enhancer-promoter loops to regulate Treg-specific gene expression. *Sci Immunol* **7**,
639 eabj9836, doi:10.1126/sciimmunol.abj9836 (2022).
640 28 Bandukwala, H. S. *et al.* Structure of a domain-swapped FOXP3 dimer on DNA and its
641 function in regulatory T cells. *Immunity* **34**, 479-491, doi:10.1016/j.immuni.2011.02.017
642 (2011).
643 29 Hill, J. A. *et al.* Foxp3 transcription-factor-dependent and -independent regulation of the
644 regulatory T cell transcriptional signature. *Immunity* **27**, 786-800,
645 doi:10.1016/j.immuni.2007.09.010 (2007).
646 30 Gavin, M. A. *et al.* Foxp3-dependent programme of regulatory T-cell differentiation.
647 *Nature* **445**, 771-775, doi:10.1038/nature05543 (2007).
648 31 Rao, S. S. P. *et al.* Cohesin Loss Eliminates All Loop Domains. *Cell* **171**, 305-320 e324,
649 doi:10.1016/j.cell.2017.09.026 (2017).
650 32 Nora, E. P. *et al.* Targeted Degradation of CTCF Decouples Local Insulation of
651 Chromosome Domains from Genomic Compartmentalization. *Cell* **169**, 930-944 e922,
652 doi:10.1016/j.cell.2017.05.004 (2017).
653 33 Fang, R. *et al.* Mapping of long-range chromatin interactions by proximity ligation-
654 assisted ChIP-seq. *Cell Res* **26**, 1345-1348, doi:10.1038/cr.2016.137 (2016).

655 34 Gilbert, L. A. *et al.* CRISPR-mediated modular RNA-guided regulation of transcription in
656 eukaryotes. *Cell* **154**, 442-451, doi:10.1016/j.cell.2013.06.044 (2013).
657 35 Leng, F. *et al.* The transcription factor FoxP3 can fold into two dimerization states with
658 divergent implications for regulatory T cell function and immune homeostasis.
659 *Immunity*, doi:10.1016/j.immuni.2022.07.002 (2022).
660 36 Weintraub, A. S. *et al.* YY1 Is a Structural Regulator of Enhancer-Promoter Loops. *Cell*
661 **171**, 1573-1588 e1528, doi:10.1016/j.cell.2017.11.008 (2017).
662
663

Methods

Mice

All mice were housed in a specific pathogen-free facility under a 12 h light/dark cycle, with an ambient temperature of 20–26 °C and humidity of 30–70% at the Salk Institute. Animal experiments were performed under the regulation of the Institutional Animal Care and Use Committee according to the institutional guidelines. All mice used in the present study are in the C57BL/6 genetic background. Rag1$^{-/-}$ mice purchased from the Jackson Laboratory were used for adoptive Treg cell transfer. Foxp3$^{Thy1.1}$ reporter mice[37], Foxp3^{GFP} reporter mice[19], and Foxp3^{GFPKO} mice[38] were used to isolate T cell populations from the thymus and Tcon and Treg cells from spleen for in-situ Hi-C, PLAC-seq, CUT&RUN, and RNA-seq experiments. Rosa-Cas9/Foxp3$^{Thy1.1}$ mice[39] were used to isolate Treg cells for CRISPR validation of the effect of Foxp3-binding sites on Helios expression.

Generation of Foxp3 domain-swap mutant knock-in mice

The Foxp3 domain-swap mutant mice were generated by CRISPR/Cas9-based genome editing[40]. Briefly, two sgRNAs containing the target sequences gRNA1(TGAAAGGGGGTCGCATATTG) and gRNA2 (AAACCACCCCGCCACCTGGA) and Cas9 protein were used to introduce double-strand DNA breaks; a 1340 base pair (bp) single-strand DNA (ssDNA) containing the sequence encoding the three amino acids mutations (W348Q, M370T, A372P) was used to introduce Foxp3 domain-swap mutations via homology-directed DNA repair mechanism. The gRNAs-Cas9 RNP together with ssDNA were injected into fertilized eggs derived from the Foxp3$^{Thy1.1}$ reporter mice, and then transplanted into pseudo-prepregnant recipient mice. The genomic region surrounding the target sites was amplified from genomic DNA of resultant founder progeny by PCR using the following primers: 5'-TCTGAGGAGCCCCAAGATGT-3', 5'-CCACTCGCACAAAGCACTTG-3'. After verifying the Foxp3 domain-swap mutations by sequencing, Foxp3 DSM mice were bred with Foxp3$^{Thy1.1}$ mice and analyzed to determine the outcomes of the Foxp3 domain-swap mutation. Details of the ssDNA sequence are listed in Supplementary Table 1.

T cell isolation and analysis

DN, DP, CD8SP, CD4SP, CD25$^+$ Treg precursor, Foxp3^{lo} Treg precursor, thymic Treg cells were isolated by FACS sorting from a thymocyte suspension. Tcon and Treg cells were isolated from the spleen by pre-enrichment with EasySep Mouse CD4+ T cell Isolation Kit (STEMCELL Technologies, Cat# 19852), and FACS sorting. The individual cell population was sorted by FACS using the following markers. DN: CD45$^+$CD4$^-$CD8$^-$; DP:CD45$^+$CD4$^+$CD8$^+$; CD8SP: CD45$^+$CD4$^-$CD8$^+$; CD4SP: CD45$^+$CD4$^+$CD8$^-$CD25$^-$ Foxp3-reporter$^-$; CD25$^+$ Treg precursor: CD45.2$^+$CD4$^+$CD8$^-$CD25$^+$Foxp3-reporter$^-$; Foxp3^{lo} Treg precursor: CD45$^+$CD4$^+$CD8$^-$CD25$^-$Foxp3-reporter^{low}; mature thymic Treg: CD45$^+$CD4$^+$CD8$^-$CD25$^+$Foxp3-reporter$^+$; Splenic Tcon cells: CD45$^+$TCRb$^+$CD4$^+$CD8$^-$ Foxp3-reporter$^-$; splenic Treg cells: CD45$^+$ TCRb$^+$CD4$^+$CD8$^-$Foxp3-reporter (Thy1.1 or GFP)$^+$.

To analyze immune cell compositions in Foxp3 DSM mice, a single cell suspension was prepared from the spleen or lymph nodes, treated with red cell lysis buffer, and filtered through 70 μm cell strainer. For transcription factor staining, cells were first stained for surface markers, followed by fixation and permeabilization with reagents from the Foxp3/Transcription Factor Staining Buffer Set (eBioscience, 00-5521-00) and incubated with antibodies according to the manufacturer's protocol. For cytokine analysis, cells were stimulated with phorbol 12-myristate 13-acetate (PMA) (50 ng ml^{-1}; Sigma), ionomycin (500 ng ml^{-1}; Sigma) and GolgiStop (BD) for 5 hours. Cells were incubated with cell surface antibodies on ice for 30 min, and then subjected to intracellular staining using Foxp3/Transcription Factor Staining Buffer Set as described above. Samples were run on a BD FACSAria II Flow Cytometer (Becton Dickinson) and data were analyzed by FlowJo software (Tree Star).

***In situ* Hi-C**

In situ Hi-C experiments were performed as previously described[2] using restriction enzyme MboI (NEB) with minor modifications. Briefly, 0.5×10^6 cells per each developmental stage from DN to mature thymic Treg cells, and 1×10^6 splenic Tcon and Treg cells were FACS-sorted and collected for individual biological replicates. Cells were

resuspended in RMPI1640 medium at a concentration of 1×10^6 cells per mL, cross-linked with 1% formaldehyde for 10 minutes at room temperature with rotating, and subsequently lysed and digested with 100 Units of MboI/1 million cells at 37 °C for 2 hours. The following steps including making of DNA ends, proximity ligation and crosslink reversal, DNA shearing and size selection, biotin pull-down and preparation for Illumine Sequencing, final amplification and purification were carried out as previously described.

CUT&RUN

CUT&RUN experiments were performed as previously described[41] with minor modifications. To avoid the potential activation of T cells by Concanavalin-A (ConA) beads in the standard protocol, we instead used a spin-down method to collect cells as previously reported[42]. Briefly, 0.5×10^6 cells per biological replicate were collected in V-bottom 96-well plate. Cells were first washed twice in Antibody Buffer (2mM EDTA, 1X EDTA-free protease inhibitors, 0.5mM spermidine, 1x permeabilization buffer from eBioscience™ Foxp3/Transcription Factor Staining Buffer Set) by centrifugation at 1900rpm for 6 min at 4°C, and then incubated with normal IgG, H3K27ac antibody, or Foxp3 antibody on ice for 1 hour. After two washes with buffer 1 (1X EDTA-free protease inhibitors, 0.5mM spermidine, 1x permeabilization buffer), cell pellets were incubated with pA/G-MNase (20X) enzyme (EpiCypher) in 50µl buffer 1 at 4°C for 1 hour. Cells were washed twice in saponin buffer (0.05% (w/v) saponin, 1X EDTA-free protease inhibitors, 0.5mM spermidine in PBS) and resuspended in 100µl calcium buffer (2mM $CaCl_2$ in buffer 2) on ice for 30 min. 100µl 2x stop buffer (20mM EDTA, 4mM EGTA in saponin buffer) was then added and incubated at 37°C for 10-20 min to release cleaved chromatin fragments. The supernatant containing chromatin fragments was collected by centrifugation and DNA was extracted using a QIAGEN MinElute kit according to manufacturer's protocol.

The CUT&RUN libraries were prepared using the NEBNext® UltraTM II DNA Library Prep Kit for Illumina® (E7645) according to manufacturer's instructions.

PLAC-seq

PLAC experiments were performed as previously described[33]. Briefly, 20×10^6 cells per biological replicate were crosslinked in 1% formaldehyde for 10 minutes at room temperature. After digestion with the restriction enzyme MboI, labeling DNA ends with biotin-14-dATP, and proximity ligation of DNA ends, the resultant chromatin was sonicated to 200-600 bp using a Covaris E229 sonicator for 10 min. Sonicated chromatin was pre-cleared with Protein A+G magnetic beads followed by overnight chromatin immunoprecipitations with 5 µg Foxp3 antibody. Libraries were prepared using NuGen Ovation Ultralow Library System V2 kit according to the manufacturer's instructions and sequenced by an Illumina HiSeq2500 sequencer.

RNA-seq

1×10^4 cells were FACS-sorted into TRIzol RNA isolation reagent (Invitrogen) and RNA was isolated according to the protocol. RNA concentration and integrity was determined by Bioanalyzer using RNA 6000 Pico Kit (Agilent). RNA-seq libraries were constructed using Illumina TruSeq Stranded mRNA kit (Illumina) following manufacturer's instructions.

Serum Immunoglobulin ELISA

Serum IgG1, IgG2c, IgM, and IgA concentrations were measured by ELISA using the SBA Clono-typing System (Southern Biotech).

Histology

For histology analysis, lung, liver, small intestine, and salivary gland tissues were fixed in 10% neutral buffer formalin, paraffin-embedded, sectioned, and stained with hematoxylin and eosin by Pacific Pathology (San Diego, CA).

In vitro culture of Treg cells

Treg cells were isolated from spleen of the Foxp3$^{Thy1.1}$ reporter mice by staining with PE-labeled Thy1.1 antibody followed by enrichment with Anti-PE magnetic beads (Miltenyi, Cat# 130-048-801). Purity of the Treg cells was confirmed to be over 95% by FACS . Treg cells were activated by plate-bound anti-CD3 and anti-CD28 antibodies in complete RPMI1640 medium containing 10% FBS, 100 U/ml Penicillin/Streptomycin, 1 X GlutaMax,

1 mM HEPES, 1 mM sodium pyruvate, 1X NEAA, 55 mM 2-mercaptoethanol, 10 mg/ml gentamycin, and IL-2 at 500 U/ml.

CRISPR knockout of Foxp3 binding sites in Ikzf2 locus

Cloning of sgRNAs into the pSIRG-NGFR vector, and retrovirus production in HEK293T cells were performed as previously described[43]. Details of sgRNA sequence are listed in Supplementary Table 2.

To test the effects of Foxp3 binding sites on Helios expression *in vitro*, Treg cells isolated from Rosa-Cas9/Foxp3$^{Thy1.1}$ mice were transduced with retrovirus carrying the sgRNAs targeting P1 region, P6 region, or control non-targeting sgRNAs. Cells were stained and analyzed for Helios expression by FACS 5 days after transduction.

***In vivo* adoptive Treg cell transfer**

To test the effect of Foxp3 binding sites in the *Ikzf2* locus on Helios expression in vivo, Treg cells from Rosa-Cas9 mice were first transduced with control sgRNAs, sgRNAs targeting P1 or P6 region on day 1, and then sorted by FACS on day 3 to enrich Treg cells transduced with sgRNAs (CD4$^+$Foxp3$^{Thy1.1+}$NGFR$^+$). CD45.2$^+$ Treg cells transduced with control sgRNAs were mixed with CD45.1$^+$CD45.2$^+$ Treg cells transduced with sgRNAs targeting P1 or P6 region respectively at a ratio of 50:50 into RAG KO mice. 2 weeks after transfer, T cells in the spleen were harvested for analysis of the expression of Helios

In-situ Hi-C and PLAC-seq data analysis

Hi-C and PLAC-seq data were aligned to the mm9 reference genome using BWA-MEM[44]. Reads were filtered (MAPQ >= 30) and paired using a previously described pipeline[45]. PCR duplicate reads were removed using Picard. Contact matrices were generated and normalized using the iterative correction method[46]. Enriched contacts in the PLAC-seq data were identified using HICCUPs[47].

To detect differential chromatin interactions between experiments, we calculated contact frequencies in 25kb bins for all interactions genome wide separated by less than 1Mb. Differential interacting regions were called using edgeR[48] with Benjamini-Hochberg correction for multiple testing.

Transcription factor motif enrichment in Foxp3-dependent chromatin interaction sites was performed by first identifying differential chromatin interactions between wild-type (Foxp3GFP+) and Foxp3 knockout (KIKO GFP+) Tregs at a resolution of 25kb. Differential interacting regions were overlapped with DNase I Hypersensitive sites in mouse Tregs from ENCODE (accession ENCFF566TDU). Motif enrichment over these DHS sites found in differential interaction regions was performed using Homer[49] using the collection of known vertebrate motifs from the JASPAR database.

RNA-seq data analysis

RNA-seq data were aligned by using STAR[44] to the mm9 reference genome. PCR duplicates were removed, and read counts were quantified over GENCODE genes (vM1) using HTSeq and subject to RPKM normalization. Differentially expressed genes were identified using edgeR[48]. Gene Ontology analysis was performed using TopGO[50].

CUT&RUN data analysis

CUT&RUN data was aligned to the mm9 reference genome using BWA-MEM[44]. Peaks were called using MACS2[51]. Peaks calls from the Foxp3 experiments together to create a union set of peaks. Using this merged peak set, we then identified differential Foxp3 sites using edgeR[48].

Data availability

The sequencing data from the RNA-seq, ChIP-seq, CUT&RUN, Hi-C, and PLAC-seq experiments have been deposited in Gene Expression Omnibus (GEO) with the following accession ID: GSE217147. [https://www.ncbi.nlm.nih.gov/geo/query/acc.cgi]. Please use the reviewer token “otkxesceztgvvkz”.

References for Methods

37 Liston, A. *et al.* Differentiation of regulatory Foxp3+ T cells in the thymic cortex. *Proc Natl Acad Sci U S A* **105**, 11903-11908, doi:10.1073/pnas.0801506105 (2008).

38 Gavin, M. A. *et al.* Foxp3-dependent programme of regulatory T-cell differentiation. *Nature* **445**, 771-775, doi:10.1038/nature05543 (2007).

39 Loo, C. S. *et al.* A Genome-wide CRISPR Screen Reveals a Role for the Non-canonical Nucleosome-Remodeling BAF Complex in Foxp3 Expression and Regulatory T Cell Function. *Immunity* **53**, 143-157 e148, doi:10.1016/j.immuni.2020.06.011 (2020).

853 40 Yang, H., Wang, H. & Jaenisch, R. Generating genetically modified mice using
854 CRISPR/Cas-mediated genome engineering. *Nat Protoc* **9**, 1956-1968,
855 doi:10.1038/nprot.2014.134 (2014).
856 41 Skene, P. J. & Henikoff, S. An efficient targeted nuclease strategy for high-resolution
857 mapping of DNA binding sites. *Elife* **6**, doi:10.7554/eLife.21856 (2017).
858 42 van der Veeken, J. *et al.* The Transcription Factor Foxp3 Shapes Regulatory T Cell Identity
859 by Tuning the Activity of trans-Acting Intermediaries. *Immunity* **53**, 971-984 e975,
860 doi:10.1016/j.immuni.2020.10.010 (2020).
861 43 Liu, Z. *et al.* Glucocorticoid signaling and regulatory T cells cooperate to maintain the
862 hair-follicle stem-cell niche. *Nat Immunol*, doi:10.1038/s41590-022-01244-9 (2022).
863 44 Li, H. Aligning sequence reads, clone sequences and assembly contigs with BWA-MEM.
864 *arXiv e-prints*, arXiv:1303.3997 (2013).
865 45 Dixon, J. R. *et al.* Integrative detection and analysis of structural variation in cancer
866 genomes. *Nat Genet* **50**, 1388-1398, doi:10.1038/s41588-018-0195-8 (2018).
867 46 Imakaev, M. *et al.* Iterative correction of Hi-C data reveals hallmarks of chromosome
868 organization. *Nat Methods* **9**, 999-1003, doi:10.1038/nmeth.2148 (2012).
869 47 Durand, N. C. *et al.* Juicer Provides a One-Click System for Analyzing Loop-Resolution Hi-
870 C Experiments. *Cell Syst* **3**, 95-98, doi:10.1016/j.cels.2016.07.002 (2016).
871 48 Robinson, M. D., McCarthy, D. J. & Smyth, G. K. edgeR: a Bioconductor package for
872 differential expression analysis of digital gene expression data. *Bioinformatics* **26**, 139-
873 140, doi:10.1093/bioinformatics/btp616 (2010).
874 49 Heinz, S. *et al.* Simple combinations of lineage-determining transcription factors prime
875 cis-regulatory elements required for macrophage and B cell identities. *Mol Cell* **38**, 576-
876 589, doi:10.1016/j.molcel.2010.05.004 (2010).
877 50 Alexa A, R. J. topGO: Enrichment Analysis for Gene Ontology. R package version 2.50.0.
878 (2022).
879 51 Zhang, Y. *et al.* Model-based analysis of ChIP-Seq (MACS). *Genome Biol* **9**, R137,
880 doi:10.1186/gb-2008-9-9-r137 (2008).
881
882

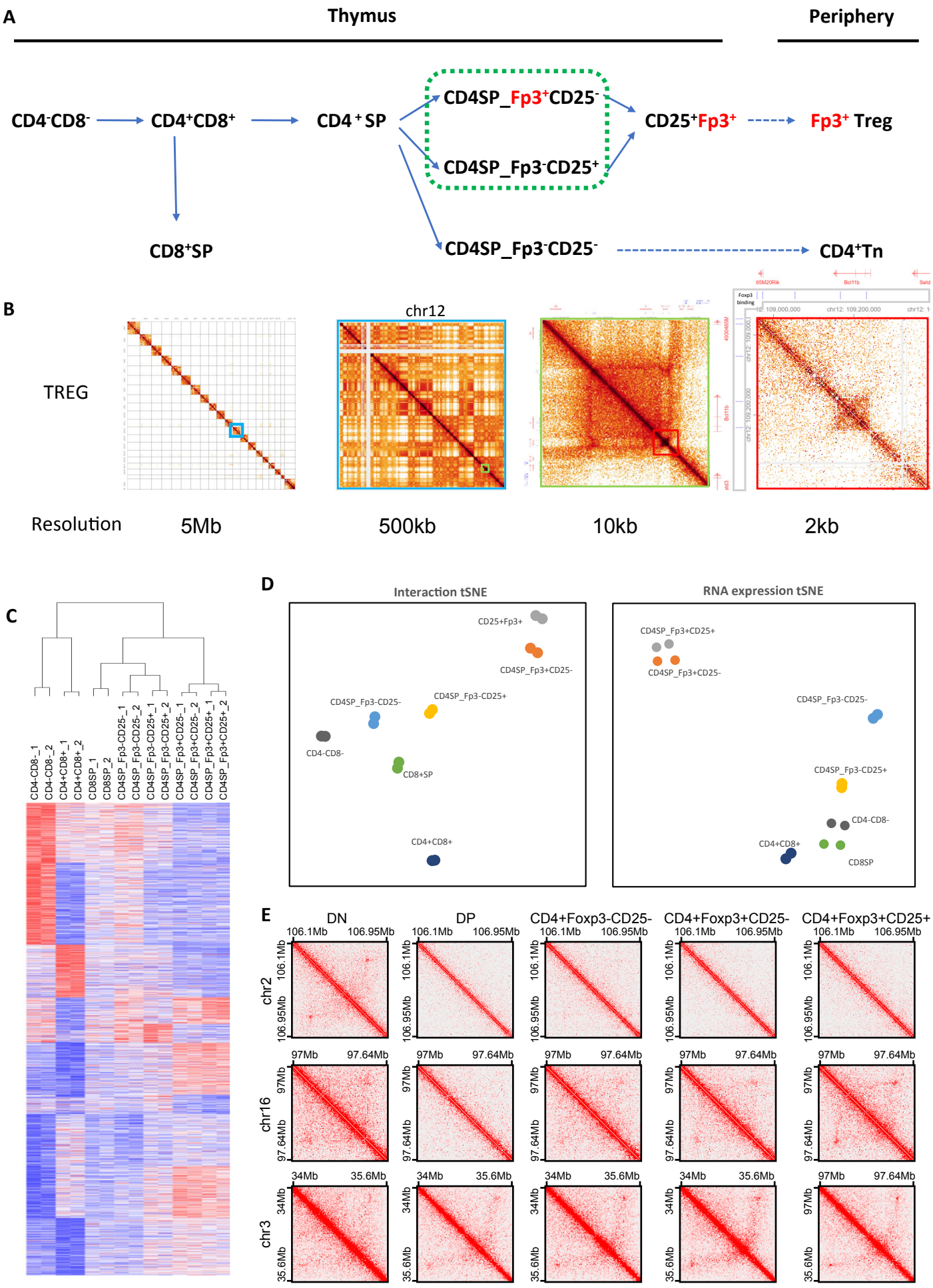
A
Thymus
Periphery
CD4-CD8-
CD4+CD8+
CD4+SP
CD4SP_Fp3+CD25-
CD4SP_Fp3-CD25+
CD25+Fp3+
Fp3+ Treg
CD8+SP
CD4SP_Fp3-CD25-
CD4+Tn
B
TREG
chr12
Resolution
5Mb
500kb
10kb
2kb
C
CD4-CD8-_1
CD4-CD8-_2
CD4+CD8+_1
CD4+CD8+_2
CD8SP_1
CD8SP_2
CD4SP_Fp3-CD25-_1
CD4SP_Fp3-CD25-_2
CD4SP_Fp3-CD25+_1
CD4SP_Fp3-CD25+_2
CD4SP_Fp3+CD25-_1
CD4SP_Fp3+CD25-_2
CD4SP_Fp3+CD25+_1
CD4SP_Fp3+CD25+_2
D
Interaction tSNE
CD25+Fp3+
CD4SP_Fp3+CD25-
CD4SP_Fp3-CD25-
CD4SP_Fp3-CD25+
CD4-CD8-
CD8+SP
CD4+CD8+
RNA expression tSNE
CD4SP_Fp3+CD25+
CD4SP_Fp3+CD25-
CD4SP_Fp3-CD25-
CD4SP_Fp3-CD25+
CD4-CD8-
CD4+CD8+
CD8SP
E
DN
DP
CD4+Foxp3-CD25-
CD4+Foxp3+CD25-
CD4+Foxp3+CD25+
chr2
chr16
chr3
106.1Mb
106.95Mb
97Mb
97.64Mb
34Mb
35.6Mb

Figure 1

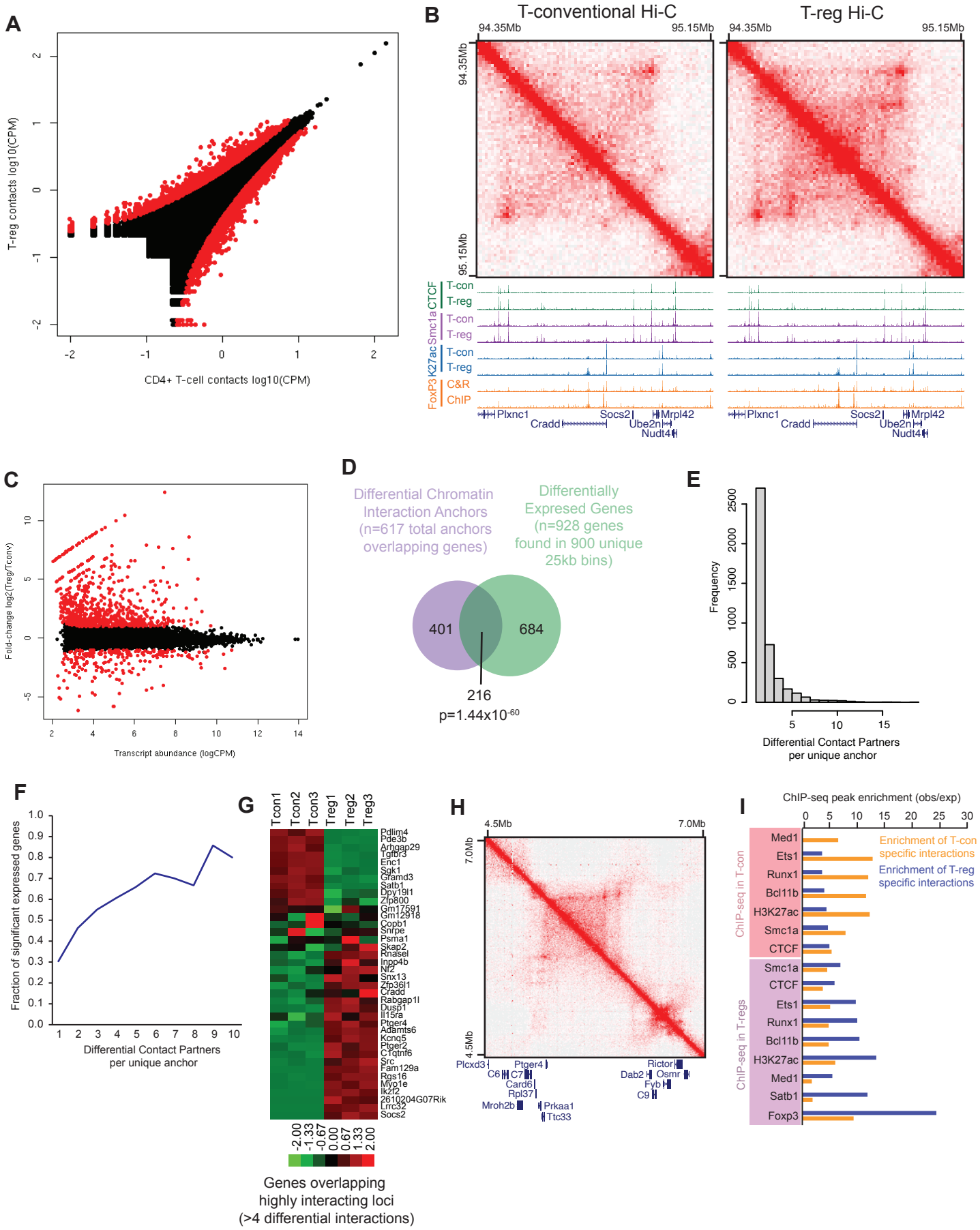
A
T-reg contacts log10(CPM)
CD4+ T-cell contacts log10(CPM)
B
T-conventional Hi-C
T-reg Hi-C
94.35Mb
95.15Mb
CTCF
Smc1a
K27ac
FoxP3
T-con
T-reg
C&R
ChIP
Plxnc1
Cradd
Socs2
Ube2n
Mrpl42
Nudt4
C
Fold-change log2(Treg/Tconv)
Transcript abundance (logCPM)
D
Differential Chromatin Interaction Anchors (n=617 total anchors overlapping genes)
Differentially Expressed Genes (n=928 genes found in 900 unique 25kb bins)
401
684
216
p=1.44x10-60
E
Frequency
Differential Contact Partners per unique anchor
F
Fraction of significant expressed genes
Differential Contact Partners per unique anchor
G
Tcon1
Tcon2
Tcon3
Treg1
Treg2
Treg3
Pdlim4
Pde3b
Arhgap29
Tgfbr3
Enc1
Sgk1
Gfamd3
Satb1
Dpy19l1
Zfp800
Gm17591
Gm12918
Copb1
Snrpe
Psma1
Skap2
Rnase1
Inpp4b
Nf2
Snx13
Zfp36l1
Cradd
Rabgap1l
Dusp1
Il15ra
Ptger4
Adamts6
Kcnq5
Ptger2
C1qtnf6
Src
Fam129a
Rgs16
Myo1e
Ikzf2
2610204G07Rik
Lrrc32
Socs2
-2.00
-1.33
-0.67
0.00
0.67
1.33
2.00
Genes overlapping highly interacting loci (>4 differential interactions)
H
4.5Mb
7.0Mb
Plcxd3
Ptger4
C6
C7
Card6
Rpl37
Mroh2b
Prkaa1
Ttc33
Rictor
Dab2
Osmr
Fyb
C9
I
ChIP-seq peak enrichment (obs/exp)
ChIP-seq in T-con
ChIP-seq in T-regs
Med1
Ets1
Runx1
Bcl11b
H3K27ac
Smc1a
CTCF
Satb1
Foxp3
Enrichment of T-con specific interactions
Enrichment of T-reg specific interactions

Figure 2

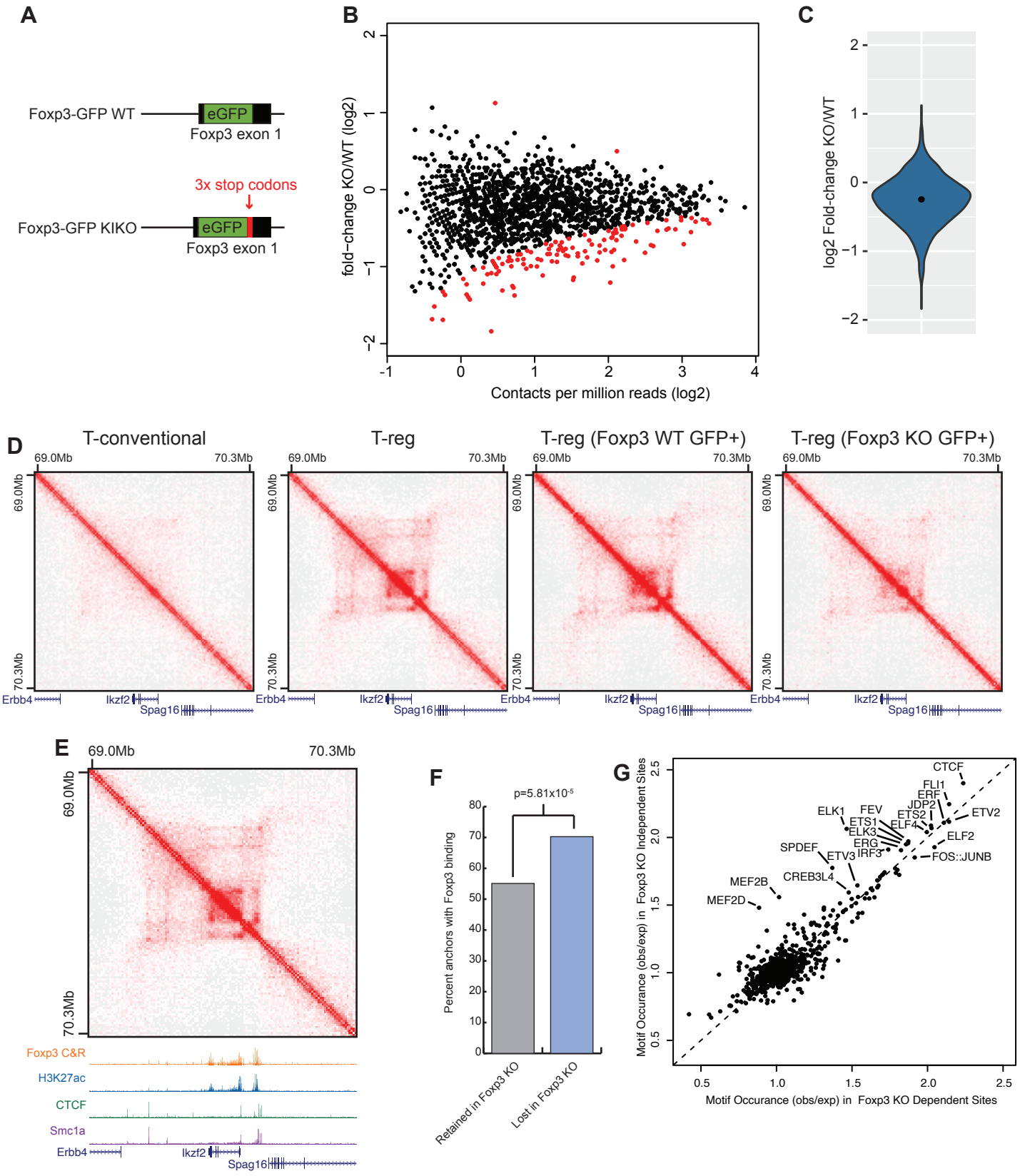
A
Foxp3-GFP WT
eGFP
Foxp3 exon 1
3x stop codons
Foxp3-GFP KIKO
eGFP
Foxp3 exon 1
B
fold−change KO/WT (log2)
Contacts per million reads (log2)
C
log2 Fold-change KO/WT
D
T-conventional
T-reg
T-reg (Foxp3 WT GFP+)
T-reg (Foxp3 KO GFP+)
69.0Mb
70.3Mb
Erbb4
Ikzf2
Spag16
E
Foxp3 C&R
H3K27ac
CTCF
Smc1a
F
p=5.81x10-5
Percent anchors with Foxp3 binding
Retained in Foxp3 KO
Lost in Foxp3 KO
G
Motif Occurance (obs/exp) in Foxp3 KO Independent Sites
Motif Occurance (obs/exp) in Foxp3 KO Dependent Sites
CTCF
FLI1
ERF
JDP2
ETS2
ETV2
ELK1
FEV
ETS1
ELF4
ELK3
ELF2
ERG
IRF3
SPDEF
ETV3
FOS::JUNB
CREB3L4
MEF2B
MEF2D

Figure 3

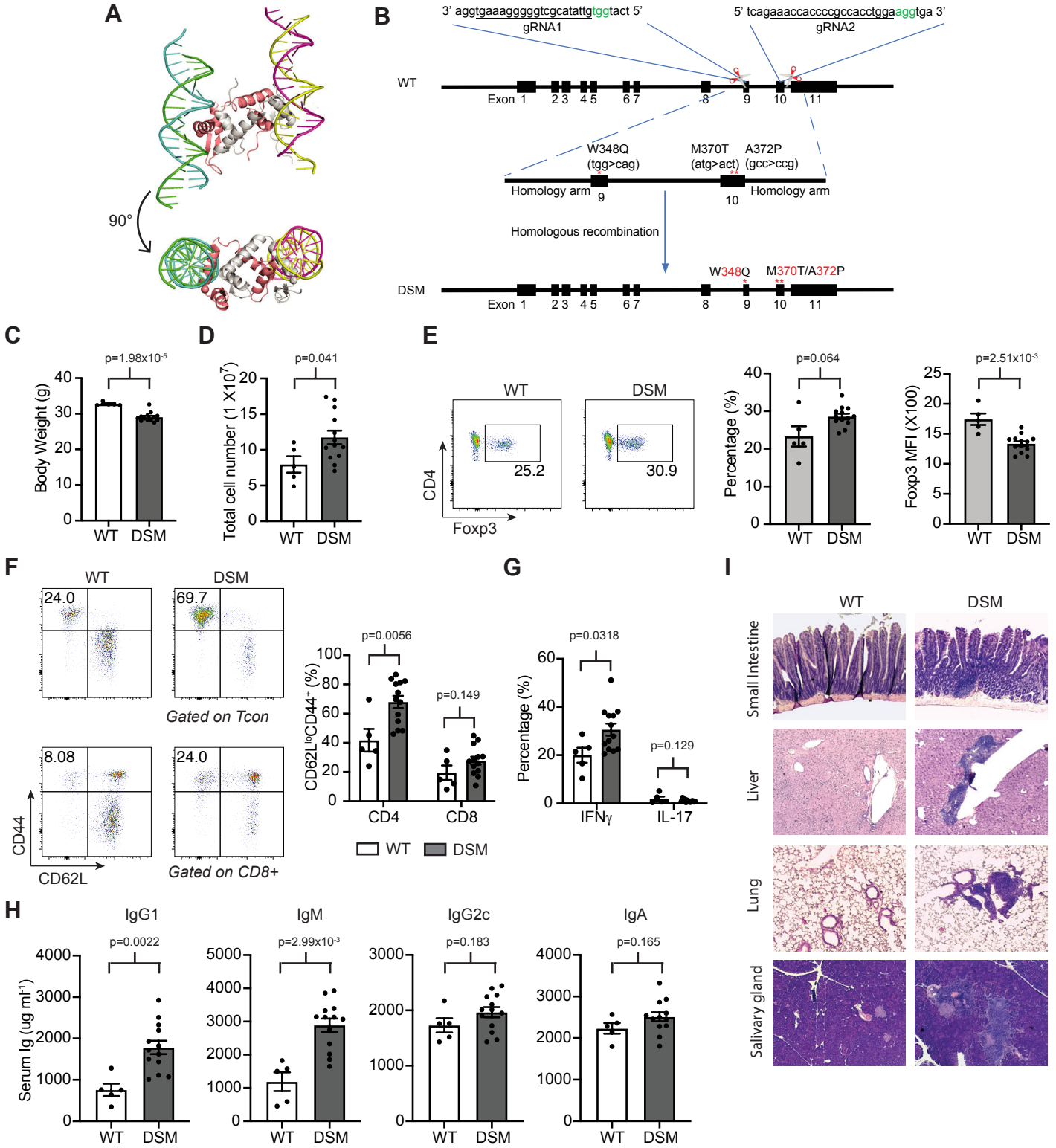
A
90°
B
3' aggtgaaagggggtcgcatattgtggtact 5'
gRNA1
5' tcagaaaccaccccgccacctggaaggtga 3'
gRNA2
WT
Exon 1
2 3
4 5
6 7
8
9
10
11
W348Q
(tgg>cag)
M370T
(atg>act)
A372P
(gcc>ccg)
Homology arm
Homology arm
Homologous recombination
DSM
W348Q
M370T/A372P
C
p=1.98x10-5
Body Weight (g)
WT
DSM
D
p=0.041
Total cell number (1 X10^7)
E
WT
DSM
CD4
Foxp3
25.2
30.9
p=0.064
Percentage (%)
p=2.51x10-3
Foxp3 MFI (X100)
F
24.0
69.7
Gated on Tcon
8.08
24.0
CD44
CD62L
Gated on CD8+
p=0.0056
p=0.149
CD62L^loCD44^+ (%)
CD4
CD8
G
p=0.0318
p=0.129
Percentage (%)
IFNγ
IL-17
I
Small Intestine
Liver
Lung
Salivary gland
H
IgG1
IgM
IgG2c
IgA
p=0.0022
p=2.99x10-3
p=0.183
p=0.165
Serum Ig (ug ml-1)

Figure 4

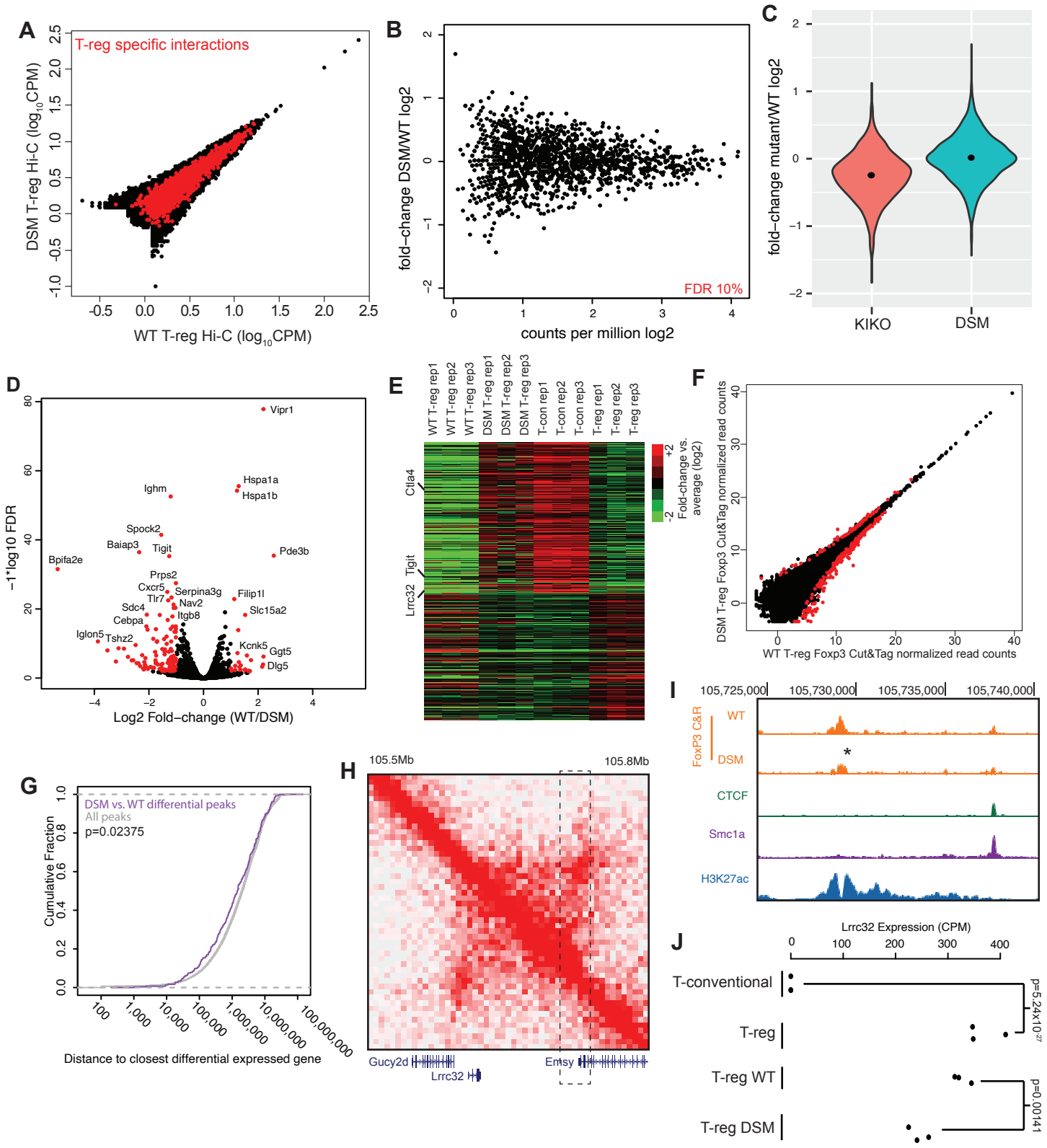
A
T-reg specific interactions
DSM T-reg Hi-C (log10CPM)
WT T-reg Hi-C (log10CPM)
B
fold−change DSM/WT log2
counts per million log2
FDR 10%
C
fold−change mutant/WT log2
KIKO
DSM
D
−1*log10 FDR
Log2 Fold−change (WT/DSM)
Vipr1
Hspa1a
Hspa1b
Ighm
Spock2
Baiap3
Tigit
Pde3b
Bpifa2e
Prps2
Cxcr5
Serpina3g
Tlr7
Nav2
Filip1l
Sdc4
Slc15a2
Cebpa
Itgb8
Iglon5
Tshz2
Kcnk5
Ggt5
Dlg5
E
WT T-reg rep1
WT T-reg rep2
WT T-reg rep3
DSM T-reg rep1
DSM T-reg rep2
DSM T-reg rep3
T-con rep1
T-con rep2
T-con rep3
T-reg rep1
T-reg rep2
T-reg rep3
Ctla4
Tigit
Lrrc32
Fold-change vs. average (log2)
F
DSM T-reg Foxp3 Cut&Tag normalized read counts
WT T-reg Foxp3 Cut&Tag normalized read counts
G
DSM vs. WT differential peaks
All peaks
p=0.02375
Cumulative Fraction
Distance to closest differential expressed gene
H
105.5Mb
105.8Mb
Gucy2d
Lrrc32
Emsy
I
105,725,000
105,730,000
105,735,000
105,740,000
FoxP3 C&R
WT
DSM
CTCF
Smc1a
H3K27ac
J
Lrrc32 Expression (CPM)
T-conventional
T-reg
T-reg WT
T-reg DSM
p=5.24x10-27
p=0.00141

Figure 5

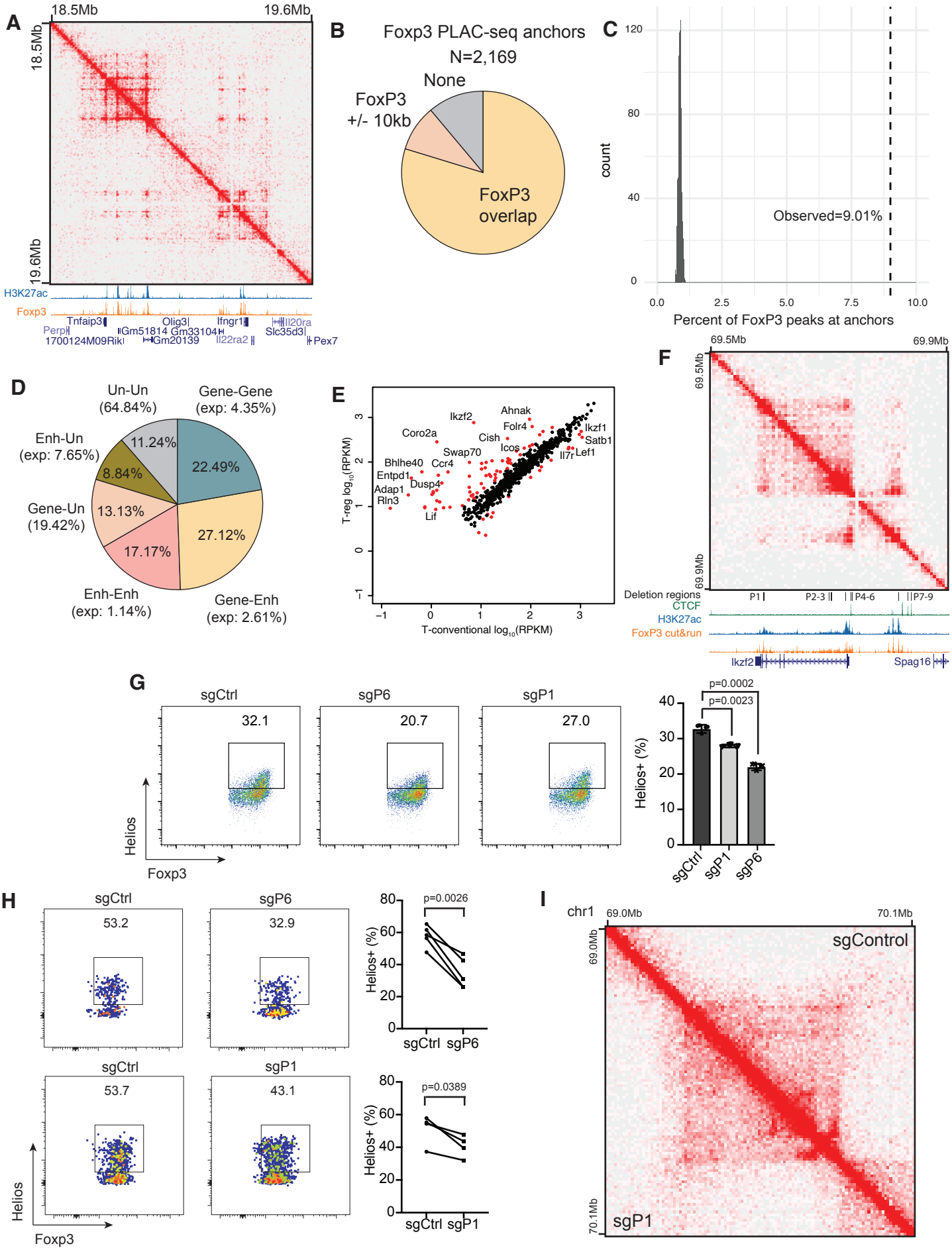
A
18.5Mb
19.6Mb
H3K27ac
Foxp3
Tnfaip3
Olig3
Ifngr1
Il20ra
Perp
Gm51814
Gm33104
Slc35d3
1700124M09Rik
Gm20139
Il22ra2
Pex7
B
Foxp3 PLAC-seq anchors
N=2,169
None
FoxP3
+/- 10kb
FoxP3
overlap
C
count
Observed=9.01%
Percent of FoxP3 peaks at anchors
D
Un-Un
(64.84%)
Gene-Gene
(exp: 4.35%)
Enh-Un
(exp: 7.65%)
Gene-Un
(19.42%)
Enh-Enh
(exp: 1.14%)
Gene-Enh
(exp: 2.61%)
11.24%
22.49%
8.84%
13.13%
27.12%
17.17%
E
T-reg log10(RPKM)
T-conventional log10(RPKM)
Ikzf2
Ahnak
Folr4
Coro2a
Cish
Ikzf1
Satb1
Swap70
Icos
Il7r
Lef1
Bhlhe40
Ccr4
Entpd1
Dusp4
Adap1
Rln3
Lif
F
69.5Mb
69.9Mb
Deletion regions
P1
P2-3
P4-6
P7-9
CTCF
H3K27ac
FoxP3 cut&run
Ikzf2
Spag16
G
sgCtrl
sgP6
sgP1
32.1
20.7
27.0
Helios
Foxp3
Helios+ (%)
p=0.0002
p=0.0023
H
53.2
32.9
53.7
43.1
p=0.0026
p=0.0389
I
chr1
69.0Mb
70.1Mb
sgControl
sgP1

Figure 6

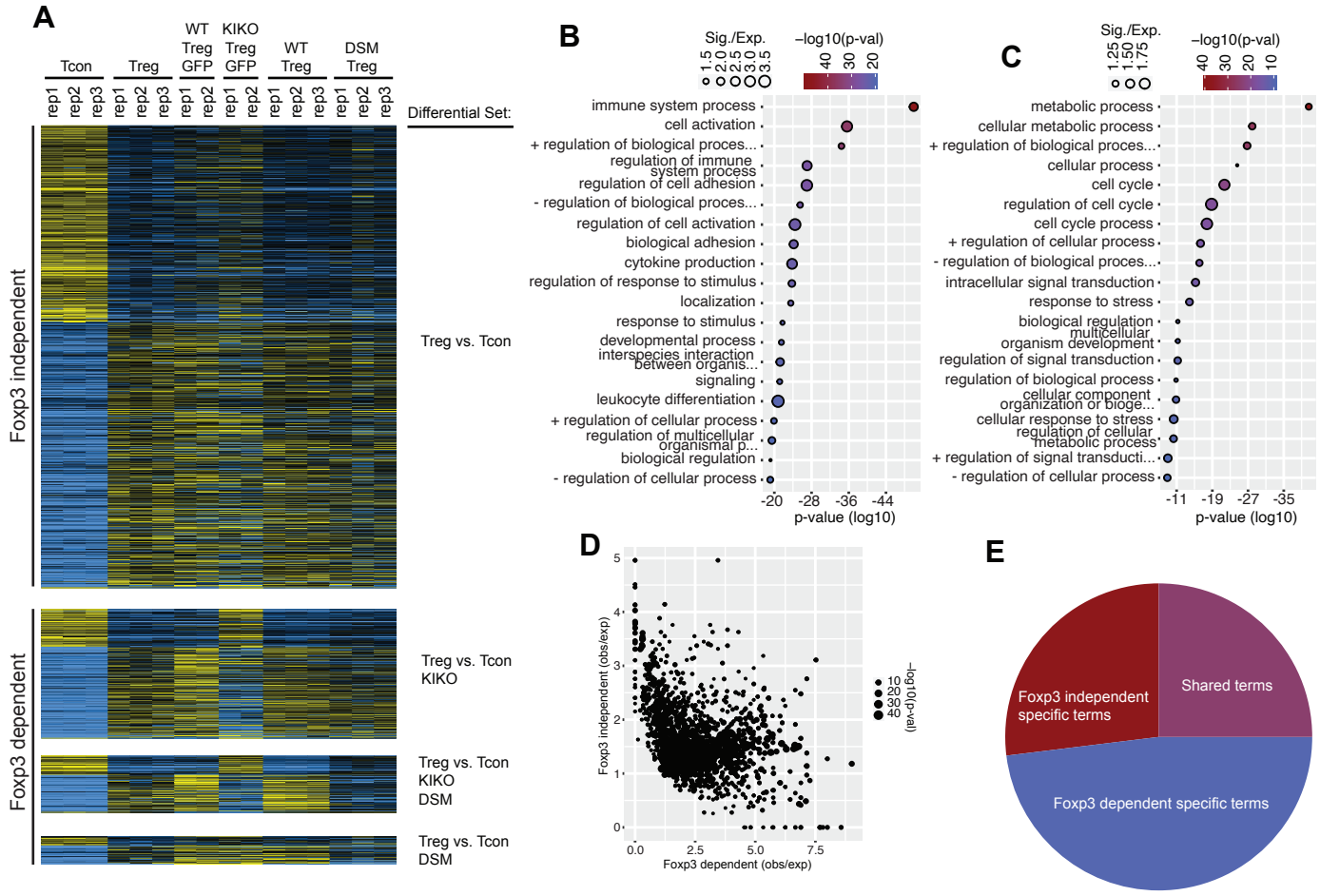
A
Tcon
Treg
WT Treg GFP
KIKO Treg GFP
WT Treg
DSM Treg
rep1 rep2 rep3
Differential Set:
Foxp3 independent
Foxp3 dependent
Treg vs. Tcon
Treg vs. Tcon KIKO
Treg vs. Tcon KIKO DSM
Treg vs. Tcon DSM
B
Sig./Exp.
–log10(p-val)
immune system process
cell activation
+ regulation of biological proces...
regulation of immune system process
regulation of cell adhesion
- regulation of biological proces...
regulation of cell activation
biological adhesion
cytokine production
regulation of response to stimulus
localization
response to stimulus
developmental process
interspecies interaction between organis...
signaling
leukocyte differentiation
+ regulation of cellular process
regulation of multicellular organismal p...
biological regulation
- regulation of cellular process
p-value (log10)
C
metabolic process
cellular metabolic process
+ regulation of biological proces...
cellular process
cell cycle
regulation of cell cycle
cell cycle process
+ regulation of cellular process
- regulation of biological proces...
intracellular signal transduction
response to stress
biological regulation
multicellular organism development
regulation of signal transduction
regulation of biological process
cellular component organization or bioge...
cellular response to stress
regulation of cellular metabolic process
+ regulation of signal transducti...
- regulation of cellular process
p-value (log10)
D
Foxp3 independent (obs/exp)
Foxp3 dependent (obs/exp)
–log10(p-val)
E
Shared terms
Foxp3 independent specific terms
Foxp3 dependent specific terms

Figure 7